Lire
la première partie
de la thèse

Chapter 8

2D Splitter Plate

Contents

8.1 Introduction

Most high-performance propulsion devices such as turbines, rocket engines or scramjets have been and are being developed through a costly trial-and-error process. The know-how accumulated over the years by designers and engineers is considerable. Nevertheless, a fundamental understanding of the mechanisms at play is necessary for further gains in performance, safety, fuel efficiency and pollutant emissions. One of the key areas for improvement is to investigate the processes through which the flame is stabilized in the combustion chamber. Indeed, flame stabilization has a direct influence on the robustness and reliability of the engine. Performance, operating range and also combustion instabilities are massively affected by the dynamics of the flame, which is driven by a large number of parameters: pressure, temperature, fuel composition and combustion regime, just to name a few.

The present chapter addresses the stabilization of a hydrogen / oxygen flame in a Liquid-fuel Rocket Engine (LRE)-like configuration. The specificity of LREs is that they operate at very high pressure for which the thermodynamic properties depart from that of an ideal gas. Indeed, beyond a certain point, called the *critical point*, of coordinates (P_c , T_c), the distinction between gaseous and liquid phases vanishes. This state of matter is called supercritical and under these conditions, phase change is replaced by a steep but continuous variation of the density and thermodynamic properties (see Chap. 3).

Significant experimental and computational efforts were conducted in earlier work, in order to understand and model flame stabilization mechanisms. However, most of these studies were conducted at atmospheric pressure, which is not representative of the operating conditions of LRE. In the case of LREs, the experiments are dissuasively expensive and the precision of modern laser diagnostics is hindered by the density gradients encountered in supercritical conditions. For these reasons, there are only a few experimental setups operating at supercritical pressure and they are facing tremendous difficulties to retrieve quantitative local properties.

The objective of this chapter is to address flame stabilization with high-fidelity numerical simulations under thermodynamic conditions that are typical of a real engine. To achieve this, Direct Numerical Simulations with detailed chemistry and conjugate heat transfer are conducted. This approach allows an accurate representation of turbulence and flame-turbulence interaction. A kinetic scheme accounting for 8 species and 12 reactions is used [Boivin 2011] as described in Chap. 7 to correctly capture the chemical structure of the flame near the wall. Finally conjugate heat transfer is mandatory to describe the heat exchange between the very low temperature (typically 100 to 150 K) propellants at injection, the burnt gases which reach temperatures as high as 3800 K, and the walls.

There is a significant body of work on flame stabilization at atmospheric pressure. Carefully instrumented experiments [Cabra 2002, Su 2006] and high-fidelity numerical simulations [Yamashita 1996, Briones 2006, Yoo 2009] have allowed significant progress. Nevertheless, there is still a controversy about the details of the mechanisms at play for turbulent flame stabilization (see [Lyons 2007] for a review on the

topic).
In the field of LREs, only a few studies address flame stabilization. On the experimental side, the Mascotte test bench operated at ONERA was instrumented with simultaneous OH PLIF and OH^* light emission [Candel 2006, Singla 2006, Singla 2007]. Close-up views of the injector revealed that the flame was stabilized near the lip and seemed to oscillate because of turbulence. On the numerical side, a few groups started investigating this issue in the late nineties [Oefelein 1998] and this effort was continued over the past ten years [Juniper 2003b, Oefelein 2005, Zong 2007]. All these studies highlighted the influence of the thickness of the lip of the injector and the associated flow dynamics.
The modeling requirements for the numerical simulation of flows under supercritical thermodynamic conditions are fairly well known [Bellan 2000]. They essentially consist in using a non-linear equation of state and a consistent modification of the thermodynamic and transport coefficients [Okong'o 2002a, Meng 2003] as described inChap. 3. As for combustion modeling, recent work on laminar and turbulent flames have proposed consistent and accurate formalisms with detailed kinetic schemes [Palle 2007, Ribert 2008, Giovangigli 2011]. However, the peculiarity of supercritical flows is that the variation of state variables and thermodynamic properties are highly non-linear, resulting in steep gradients that require very fine grid resolutions. Recent work at IMFT and CERFACS [Schmitt 2010b, Ruiz 2011d] has shown that this issue may be one of the weak points of most studies of supercritical flows.

8.2 Configuration

The configuration chosen for the DNS study is a LOx/GH2 coaxial injector, representative of an injector of a LRE. Figure 8.1 gives a sketch of the numerical domain and the injection flow parameters. For CPU reasons, only 2D DNS were performed in this work. Indeed, the resolution required for a five lip thickness span-wise 3D DNS would result in a 25 billion cell mesh not available at the time of the simulations. Still it has been for long recognized that 2D DNS gives useful informations in such simple flame configuration and for the purpose of the thermal study. However results obtained here will need to be confirmed in full 3D cases. These numerical simulations are DNS in the sense that both turbulence, and combustion are fully resolved.

8.2.1 Mesh, Injection & Boundary conditions

The flow and thermodynamic conditions are chosen to be representative of a real engine under steady operation: both fuel (hydrogen) and oxidizer (oxygen) are above their critical pressure.

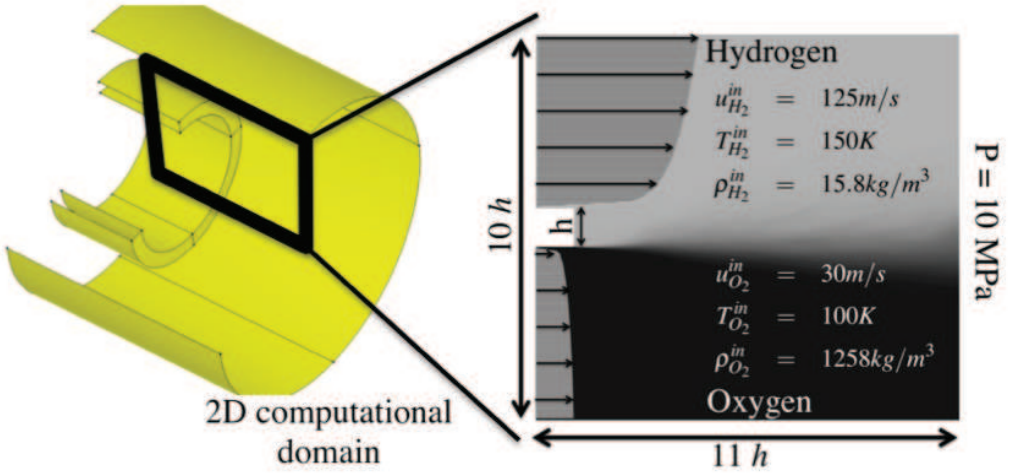

Figure 8.1: Computational domain and injection parameters. [Ruiz 2011b]

The computational domain, presented in Fig. 8.1, is 5.5 mm long in the x-direction and 5.0 mm wide in the y-direction. The splitter-plate height is $h = 0.1$ mm, and the simulation length is $L = 0.5$ mm. The mesh resolution is $\Delta = 1$ μm in a 1.5 mm layer around the splitter. Outside this zone, a transverse stretching factor of approximately 1.02 is employed. The mesh contains approximately 12 million hexahedral cells. [Ruiz 2012] has demonstrated that this resolution is sufficient to resolve the turbulent length scale down to the Kolmogorov scale.
Hydrogen is injected above the splitter at a temperature $T^{in}_{H_2} = 150$ K and a bulk

velocity $\bar{U}_{H_2} = 125$ m/s. Below the splitter, oxygen is fed at $T^{in}_{O_2} = 100$ K and $\bar{U}_{O_2} = 30$ m/s. These conditions, summarized in Tab. 8.1, were chosen to mimic a typical liquid rocket engine, at the nominal operating point. A 1/7th power law, given in Eq. 8.1 is used to mimic the mean turbulent velocity profile in a pipe flow.

$$u(y) = \bar{U} \left(\frac{y - y_w}{4.5\ h} \right)^{1/7} \tag{8.1}$$

with $\bar{U}$ the bulk velocity and $y - y_w$ the distance to the injector wall.

The outlet boundary condition is derived from the NSCBC technique [Poinsot 1992, Baum 1995] and accounts for both real-gas effects [Okong'O 2002b] and transverse terms [Lodato 2008].
With a procedure similar to that of [Bogey 2011], a sponge layer of thickness 0.5 mm is imposed at the exit of the computational domain to prevent spurious oscillations when strong density gradients hit the boundary. The upper and lower boundaries are treated as symmetries while the splitter is a no-slip wall.
No synthetic turbulence is added to the inflow boundary conditions as strong turbulence levels are generated by vortex shedding at the angles of the splitter plate. This allows the development of a reactive turbulent mixing layer downstream of the lip. A strong flame/turbulence interaction occurs then in the wake of the splitter plate, modifying flame characteristics, structure and position.

Variable		[Dimension]	$\mathbf{O_2}$	$\mathbf{H_2}$
Temperature	T	K	100	150
Density	ρ	kg.m^{-3}	1258	15.8
Velocity	$\bar{U}$	m.s^{-1}	30	125
Viscosity	μ	Pa.s	$1.69\ 10^{-4}$	$6.09\ 10^{-6}$
Sound speed	c	m.s^{-1}	877	1075
Mach number	M	-	0.034	0.116
Reynolds number	Re	-	$9.9\ 10^{4}$	$1.5\ 10^{5}$
Momentum Flux	J	kg.m^{-1}.s^{-2}	$1.132\ 10^{6}$	$2.468\ 10^{4}$

Table 8.1: Injection properties.

Several characteristic scales and non-dimensionalized quantities are given in Tab. 8.2. The reduced temperature and pressure indicate the thermodynamic conditions.
The LOx stream is in transcritical condition ($p_r > 1$; $T_r < 1$) while the H_2 stream is supercritical ($p_r > 1$; $T_r > 1$) resulting in a very large density ratio R_ρ. This will play an important role in the turbulent mixing and combustion.
Boundary conditions for the solid are treated using a Neumann condition for the coupled walls as in Chap. 6. At the bottom of the injector the temperature is assumed constant and a linear profile ranging from 100 K on the LOx side to 150 K on the GH_2 side.

Variable		$\mathbf{O_2}$	$\mathbf{H_2}$
Reduced Temperature	T_r	0.65	4.55
Reduced Pressure	p_r	2.0	7.8
Density Ratio	R_ρ	80	
Momentum Ratio	J	0.2	
Velocity Ratio	R_U	4.2	

Table 8.2: Injection characteristics.

Parameters	H2	O2	H2O	O	H	OH	H2O2	HO2
T_c (K)	33.3	154.6	647.1	105.3	190.8	105.3	141.3	141.3
P_c (MPa)	1.28	5.04	22.06	7.09	31.01	7.09	4.79	4.79
V_c (cm^3/mol)	64.3	73.4	55.9	41.2	17.1	41.2	81.9	81.9
ω_{ac}	-0.216	0.0222	0.3443	0.0	0.0	0.0	0.0	0.0
Sc	0.28	0.99	0.77	0.64	0.17	0.65	0.65	0.65

Table 8.3: Species critical-point properties (temperature T_c, pressure P_c, molar volume V_c and acentric factor ω_{ac}) and Schmidt numbers Sc.

8.2.2 Thermodynamic properties

Real-gas thermodynamics are accounted for through the Peng-Robinson equation of state [Peng 1976] as in Eq. 3.13. Transport coefficients are modeled based on the theory of corresponding states for the dynamic viscosity and the thermal conductivity [Chung 1984] as described in Chap. 3 and constant Schmidt numbers (cf. Tab. 8.3). The critical-point coordinates of the combustion intermediate species OH, O, H, H2O2 and HO2, for which no experimental data is available, is estimated using the Lennard-Jones potential-well depth σ_i, and the molecular diameter ϵ_i of the i-th species from the CHEMKIN transport coefficients of the San Diego Mechanism [Saxena 2006], according to the following expression [Giovangigli 2011]

$$V_{c,i} = 3.29 \mathcal{N}_A \sigma_i^3 \tag{8.2}$$

$$T_{c,i} = 1.316 \frac{\epsilon_i}{k_B} \tag{8.3}$$

where $\mathcal{N}_A$ is the Avogadro number and k_B is the Boltzmann constant.

This overall numerical and modeling methodology has already been validated for non reacting flows [Schmitt 2010b, Ruiz 2014]

8.3 The heat transfer problem

The main goal of this study is to calculate the thermal behavior of a H_2 / O_2 injector lip in a rocket engine configuration. Indeed, evidence of thermal fatigue has been observed in real systems, and represents an important constraint for the design.

The splitter receives fluxes from the gaseous H_2 and the liquid O_2 streams on the side and from the flame at the front face. Thermal conductivity, density and thermal capacity at constant volume of the solid material then determine the temperature field.

8.3.1 Thermal balance

On a first approach the splitter may be viewed as a simple fin. A flux balance allows to obtain the steady temperature distribution in an elementary fin surface. A simple sketch of the configuration is given in Fig. 8.2.

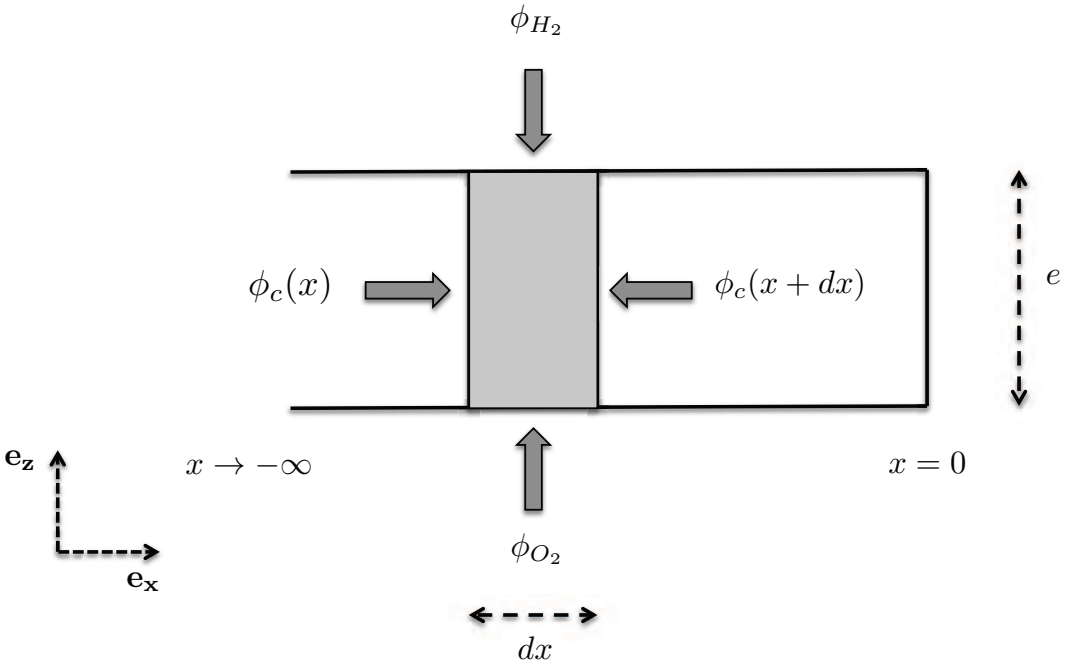

Figure 8.2: Heat fluxes in an elementary surface. ϕ_c is for conductive flux.

For a steady state, the sum of fluxes is equal to zero thus we can write:

$$\sum_k \phi_k = 0 \tag{8.4}$$

and by expressing each flux:

$$\phi_c(x) = -e\lambda \left.\frac{\partial T}{\partial x}\right|_x \tag{8.5}$$

$$\phi_c(x+dx) = e\lambda \left.\frac{\partial T}{\partial x}\right|_{x+dx} \tag{8.6}$$

$$\phi_{H_2} = h_{H_2}\left(T_{H_2} - T(x)\right) dx \tag{8.7}$$

$$\phi_{O_2} = h_{O_2}\left(T_{O_2} - T(x)\right) dx \tag{8.8}$$

where h_{H_2} (h_{O_2}) is the convective heat coefficient of H_2 (resp. O_2).
Hence we obtain:

$$e\,\lambda\left[-\left.\frac{\partial T}{\partial x}\right|_x + \left.\frac{\partial T}{\partial x}\right|_{x+dx}\right] - dx\cdot\left[h_{H_2}\left(T(x)-T_{H_2}\right) + h_{O_2}\left(T(x)-T_{O_2}\right)\right] = 0$$

$$\frac{\left.\frac{\partial T}{\partial x}\right|_{x+dx} - \left.\frac{\partial T}{\partial x}\right|_x}{dx} - \frac{h_{H_2}+h_{O_2}}{e\,\lambda}\cdot\left[T(x) - T_{H_2}\cdot\frac{h_{H_2}}{h_{H_2}+h_{O_2}} + T_{O_2}\cdot\frac{h_{O_2}}{h_{H_2}+h_{O_2}}\right] = 0$$

and finally when dx tends to 0:

$$\left.\frac{\partial^2 T}{\partial x^2}\right|_x - \frac{\overline{h}}{e\,\lambda}\Big(T(x) - \overline{T}\Big) = 0 \tag{8.9}$$

where

$$\begin{cases} \overline{h} = h_{H_2} + h_{O_2} \\ \\ \overline{T} = T_{H_2}\cdot\dfrac{h_{H_2}}{h_{H_2}+h_{O_2}} + T_{O_2}\cdot\dfrac{h_{O_2}}{h_{H_2}+h_{O_2}} \end{cases}$$

We can now set a new variable $\theta(x) = T(x) - \overline{T}$, so that Eq. 8.9 becomes:

$$\left.\frac{\partial^2 \theta}{\partial x^2}\right|_x - m^2\theta(x) = 0 \tag{8.10}$$

where

$$m = \sqrt{\frac{\overline{h}}{e\,\lambda}} \tag{8.11}$$

The homogeneous solution of Eq. 8.10 is given by

$$\theta(x) = \mathrm{A}e^{mx} + \mathrm{B}e^{-mx} \tag{8.12}$$

Boundary conditions are then used to determine the integration constant A and B values and solve the problem.

8.3.2 Dirichlet boundary conditions

To find the integration constants, a temperature T_{eq} representative of the gas mixture is imposed at the front of the splitter plate:

$$\begin{cases} T = \overline{T} \text{ when } x \to -\infty \\ \\ T = T_{eq} \text{ when } x = 0 \end{cases}$$

This leads to:

$$\begin{cases} \theta = 0 \text{ when } x \to -\infty \\ \\ \theta = \theta_{eq} \text{ when } x = 0 \end{cases}$$

Finally we can write:

$$T(x) = \overline{T} + (T_{eq} - \overline{T})\, e^{mx} \tag{8.13}$$

8.3.3 Neumann boundary conditions

Another boundary condition to evaluate the penetration length in the solid is a `Neumann` type condition where the heat flux is imposed at the tip of the splitter plate. Thus boundary conditions become

$$\begin{cases} T = \overline{T} \text{ when } x \to -\infty \\ \\ \lambda \left.\dfrac{\partial T}{\partial x}\right|_{x=0} = \Phi \text{ where } \Phi \text{ is the heat flux received by the solid} \end{cases}$$

This leads to :

$$\begin{cases} \theta = 0 \text{ when } x \to -\infty \\ \\ \lambda \left.\dfrac{\partial \theta}{\partial x}\right|_{x=0} = \Phi \end{cases} \tag{8.14}$$

Using these conditions we obtain

$$\begin{aligned} \theta &= A e^{mx} \\ \\ \frac{\partial \theta}{\partial x} &= A\, m\, e^{mx} \end{aligned}$$

Finally using Eq. 8.14 it comes

$$\theta = \frac{\phi}{\lambda\, m}\, e^{mx}$$

and we end with

$$T = \overline{T} + \frac{\phi}{\lambda\, m}\, e^{mx} \tag{8.15}$$

8.3.4 Convection coefficients

In order to evaluate the convection coefficient h in each fluid, we need to calculate the Nusselt number for both sides of the splitter. A correlation extracted from [Dittus 1930] has been used, where the Nusselt number is expressed as

$$Nu = 0.027 \cdot Re^{0.8} \cdot Pr^{0.4} \tag{8.16}$$

where Re $= Ue/\nu$ is the Reynolds number and Pr $= C_p\mu/\lambda$ is the Prandtl number.

8.4 Theoretical Results

The analytical resolution presented in Sec. 8.3 is now applied to the present splitter plate. Table 8.4 summarizes all parameters and non-dimensional numbers for the considered case.

Variable	[Dimension]	$\mathbf{O_2}$ stream	$\mathbf{H_2}$ stream
C_p	J.kg^{-1}.K^{-1}	1.89 10^3	1.62 10^4
μ	Pa.s	1.69 10^{-4}	6.09 10^{-6}
λ_g	W.m^{-1}.K^{-1}	0.0944	0.1040
Re	-	1.52e+05	1.20e+06
Pr	-	1.693	0.941
Nu	-	330	364
h	W.m^{-2}.K^{-1}	338921	379033

Table 8.4: Fluid properties & parameters using NIST database [Lemmon 2009] for the splitter case.

The solid properties are as follow:

$$\begin{cases} \lambda_s \sim 10 \text{ W.m}^{-1}\text{.K}^{-1} \\ e = 0.1 \text{ mm} \end{cases}$$

This gives the solution parameters:

$$\begin{cases} \overline{h} & = 2.00 \cdot 10^5 \text{ W.m}^{-2}\text{.K}^{-1} \\ \overline{T} & = 84.9 \text{ K} \end{cases}$$

8.4.1 Dirichlet boundary conditions

Assuming that 10% of the lip is in contact with the flame, which temperature is T_f, and 90% is in contact with a mixture of burnt gases and cold reactants at temperature T_m, we can calculate an equivalent temperature as $T_{eq} = 0.1 \cdot T_f + 0.9 \cdot T_m$. T_f have been chosen equal to the H_2/O_2 adiabatic flame temperature (3100 K) but T_m is still undetermined. Eq. 8.13 has been plotted in Fig. 8.3, with $T_m = 150$ K

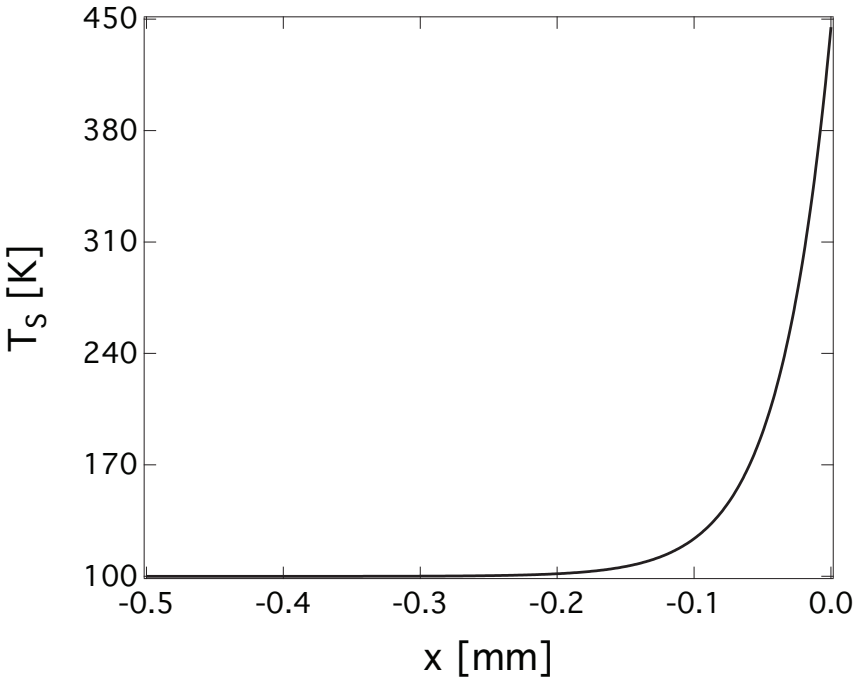

Figure 8.3: Temperature profile along the 1D splitter. Dirichlet boundary condition with $T_{eq} = 445K$

leading finally to $T_{eq} = 445$ K. The final temperature $\overline{T}$ is reached very soon in the solid.

This leads to a penetration length L_p, defined by the location where the temperature $T(x)$ reaches $1.1\,\overline{T}$ of $\sim 1.3\,e$. As T_{eq} is an uncertain quantity , a sensitivity analysis has been conducted. Table 8.5 and Fig. 8.4 show the penetration length (expressed as a multiple of the lip thickness e) as a function of the equivalent temperature T_{eq} imposed at the front face of the splitter.

The penetration length increases non-linearly with T_{eq}, but never exceeds $2.2e$, even if the flame (ie. hot gases) cover the whole front surface of the splitter ($T_{eq} > 3000$ K), ie. T_{eq} is maximum.

Equivalent Temperature T_{eq} (K)	Penetration Length L_p (e)
300	1.1211
450	1.3313
515	1.3914
650	1.5015
965	1.6717
1280	1.7818
1550	1.8619
2180	2.002
3170	2.1421

Table 8.5: Penetration length as a function of the equivalent front face temperature T_{eq}.

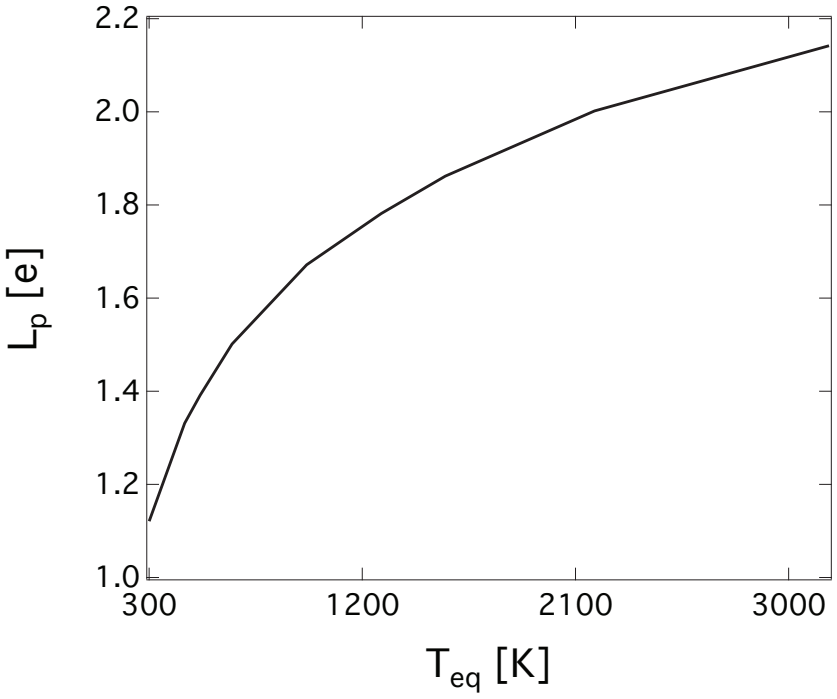

Figure 8.4: Penetration length in the splitter as a function of the equivalent temperature T_{eq} at the front face of the splitter.

8.4.2 Von Neumann boundary conditions

In order to evaluate the order of magnitude of ϕ the heat flux at the front of the splitter plate, one characteristic length and two temperatures are needed. The premixed flame thickness δ_f is chosen as a reference length, the adiabatic flame temperature T_{adia} and the front wall temperature T_p to evaluate the heat flux:

$$\phi = \lambda \left.\frac{\partial T}{\partial x}\right|_{x=0} \quad \Rightarrow \quad \sim \lambda_g \frac{\Delta T}{\delta l} \quad \Rightarrow \quad = \lambda_g \frac{T_{\text{adia}} - T_p}{\delta_f}$$

where λ_g is the thermal conductivity of the gas (typically $\sim 0.1\,\text{W.m}^{-1}\text{.K}^{-1}$).
The front wall temperature is:

$$T_p = T(x=0) = \overline{T} + \frac{\phi}{\lambda\, m} \tag{8.17}$$

By reporting the flux in Eq. 8.17, one obtains:

$$T_p = \frac{T_{\text{adia}} \frac{\lambda_g}{\delta_f} + \overline{T} \lambda\, m}{\lambda\, m + \frac{\lambda_g}{\delta_f}} \tag{8.18}$$

Taking with $T_{\text{adia}} = 3100$ K and $\delta_f = 10^{-5}$ m, the solution parameters finally writes:

$$\begin{cases} T_p & = T(x=0) = 357\text{ K} \\ \phi & = 6.89 \cdot 10^7\text{ W.m}^{-2} \end{cases} \tag{8.19}$$

Figure 8.5 shows the temperature field solution. The penetration length is now:

$$L_p = 1.22\, e \tag{8.20}$$

The value of the front lip temperature $T_p = 357$ K may seem low in regard to the large flame power but is consistent with the result obtained by [Juniper 2001] at around 300 K.

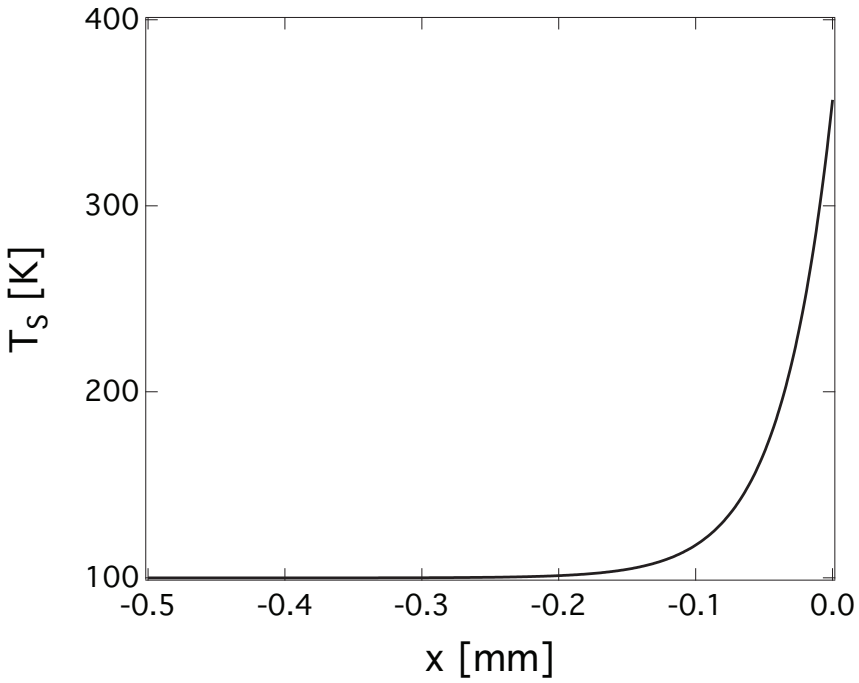

Figure 8.5: Temperature profile along the 1D splitter. Neumann boundary condition with $\phi = 6.89\,10^7$ W.m^{-2}

8.5 Reactive LES Results

In this section we present results obtained with the coupled framework developed in Chap. 4. Because the characteristic times of heat transfer in the fluid and the solid are separated by orders of magnitude, as a first step, the problem is considered quasi-steady: the solid is only sensitive to the mean flux from the fluid and filters out high-frequency oscillations. As described by [Duchaine 2009a], it is possible, in this case, to speed-up the convergence of the coupled simulation by desynchronizing the time scales in the two codes. In the present simulations, the coupling interval corresponds to $11 \cdot 10^{-6}$ s in the solid and $1.25 \cdot 10^{-9}$ s in the fluid. To avoid interpolation error, the spatial resolution in the solid is identical to that in the fluid ($\Delta = 1$ μm). This leads to cell size smaller than necessary, but the computational time for the resolution of the solid remains negligible: 1021 CPUs are used for the fluid and only 2 for the solid. One CPU is also dedicated to the scheduling of the coupled application.

For comparison reasons, the same case has been computed with an adiabatic boundary condition at the wall.

The detailed analysis of the turbulent flame can be found in [Ruiz 2011d, Ruiz 2012] and is not regarded here. Focus is made on the injector zone. As illustrated in Fig. 8.6 diffusion flame develops under near-stoichiometric conditions and the flame develops between the two propellants in the wake of the LOx-post lip. The iso-stoichiometric surface around which the flame grows, is located close to the dense oxygen jet because little gaseous oxygen is available. By transferring heat to the dense LOx stream, the flame helps generating gaseous oxygen.

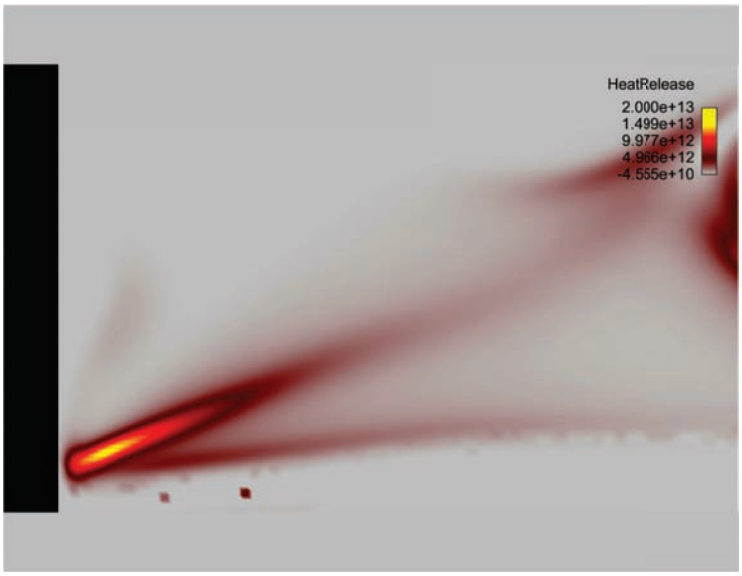

Figure 8.6: Instantaneous field of heat release rate. Zoom on the splitter plate region.

8.5.1 Flame structure

The flame is classically described with a mixture fraction, Z_H, based on the conservation of the H-atom:

$$Z_H = W_H \left(2\frac{Y_{H_2}}{W_{H_2}} + \frac{Y_H}{W_H} + 2\frac{Y_{H_2O}}{W_{H_2O}} + \frac{Y_{HO}}{W_{HO}} + \frac{Y_{HO_2}}{W_{HO_2}} + 2\frac{Y_{H_2O_2}}{W_{H_2O_2}} \right) \tag{8.21}$$

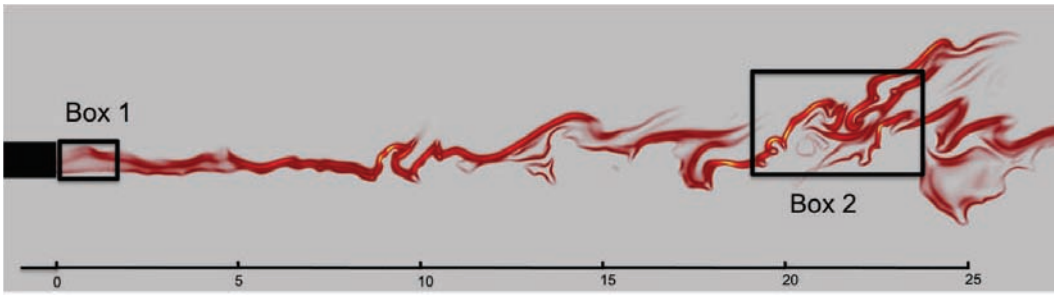

Figure 8.7: Instantaneous field of heat release rate. The boxes represent two different zones used for the scatter plots.

Scatter plots of temperature, heat release rate and species mass fractions in mixture fraction space are presented in Figs. 8.8 to 8.12 in two regions, which are highlighted by square boxes in Fig. 8.7. These plots correspond to one instantaneous flow solution.

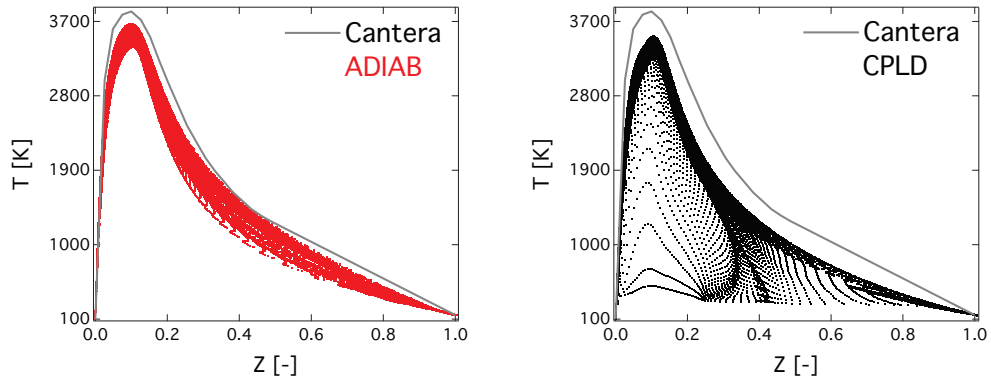

(a) Adiabatic Case

(b) Coupled Case

Figure 8.8: Scatter plot of the temperature vs. mixture fraction in the splitter configuration. Box 1.

Box 1 extends from the splitter to 0.2 mm downstream (Fig. 8.8). This is the flame anchoring region. For the adiabatic boundary condition (Fig. 8.8,a) the temperature scatter plot shows that there are no points on the mixing line,

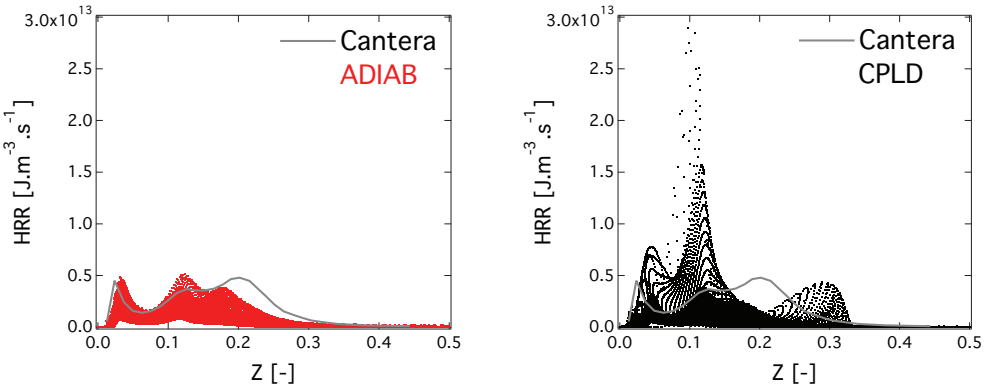

(a) Adiabatic Case (b) Coupled Case

Figure 8.9: Scatter plot of the Heat Release Rate vs. the mixture fraction in the splitter configuration. Box 1.

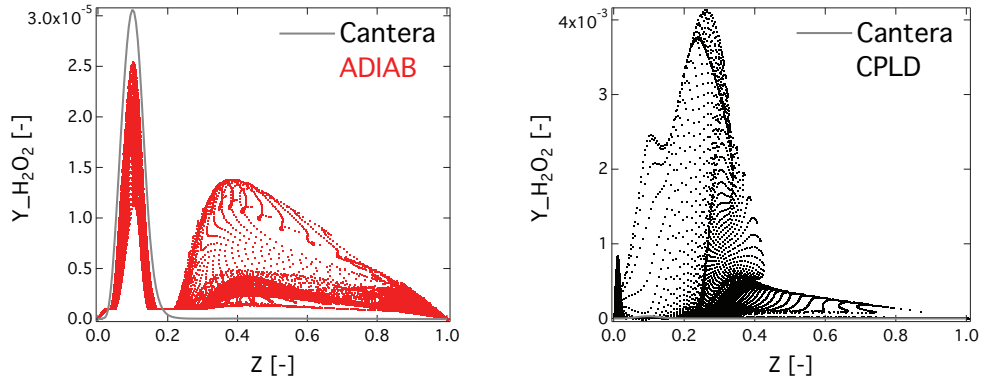

(a) Adiabatic Case (b) Coupled Case

Figure 8.10: Scatter plot of the H_2O_2 radical vs. the mixture fraction in the splitter configuration. Box 1.

indicating that the flame is ignited everywhere and no premixing occurs. The broadening of the temperature versus mixture fraction is caused by variable stretch rates and finite-rate chemistry. The grey line represents a counterflow diffusion flame at 100 bar and 300 K computed with CANTERA with a strain of $a = 2\,10^4$ s^{-1}. The heat release rate in Fig. 8.9 peaks at the stoichiometric mixture fraction ($Z_H = 0.11$) with a value of $\sim 5\,10^{12}$ J.m^3.s^{-1}, which is consistent with a diffusion flame structure, but also around $Z_H = 0.03$ *i.e.* in very lean conditions. This flame structure is very peculiar and it has been demonstrated by [Mari 2012] that it corresponds to chemical activity between burnt gases and pure oxygen.

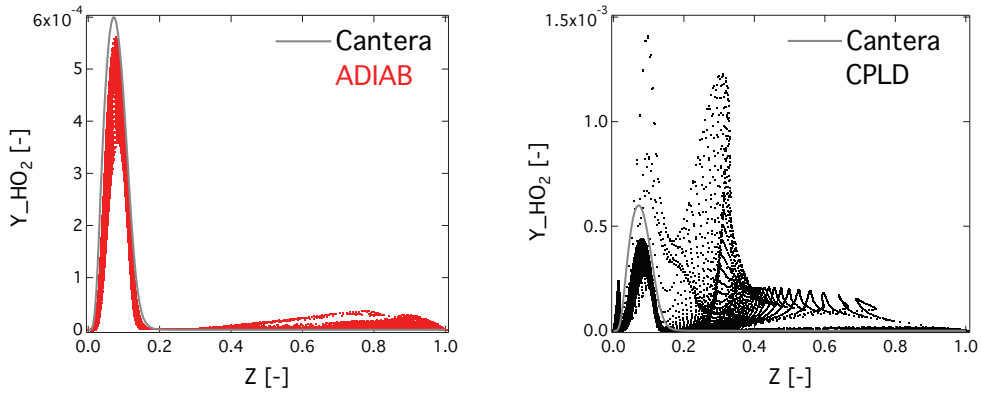

(a) Adiabatic Case (b) Coupled Case

Figure 8.11: Scatter plot of the HO_2 radical vs. the mixture fraction in the splitter configuration. Box 1.

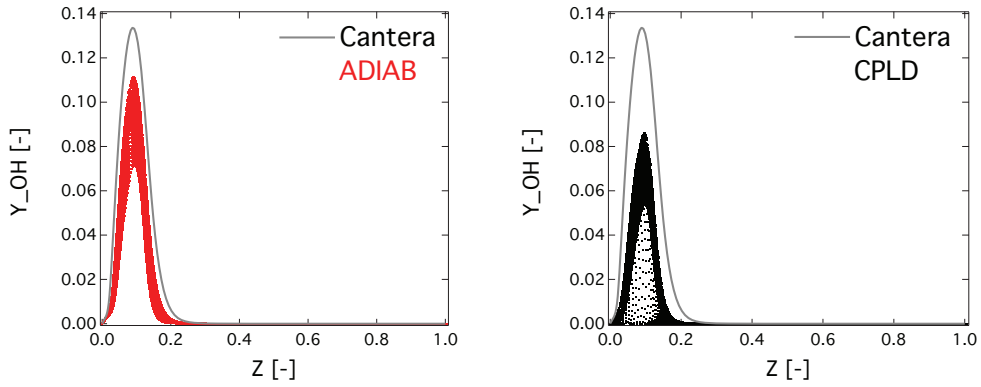

(a) Adiabatic Case (b) Coupled Case

Figure 8.12: Scatter plot of the OH radical vs. the mixture fraction in the splitter configuration. Box 1.

The coupled case scatter plots show major differences. The maximum temperature is lower than in the adiabatic case demonstrating the effect of the heat loss at the tip of the injector. Points are scattered in the whole domain which highlights premixing phenomenon due to the heat loss at the wall. Still, the heat release rate maximum value is almost one order of magnitude higher than in the adiabatic case ($\sim 3\,10^{13}$), but, as exhibited in Chap. 7 this is due to the low temperature at the wall enhancing reactions with low or zero activation energy involving radicals such as HO_2 or H_2O_2 at the wall. As shown in Fig. 8.10 the production of H_2O_2 is much higher in the coupled case. Same

conclusions can be made for HO_2 radical as shown in Fig. 8.11.

On the contrary the production of OH is little modified. In the coupled case the maximum level is only slightly lower than in the adiabatic case. OH radical production reactions have a non-zero energy of activation which implies that close to a cold wall reactions producing OH vanish, leading to a lower OH concentration. This is also consistent with the observations made in Chap. 7.

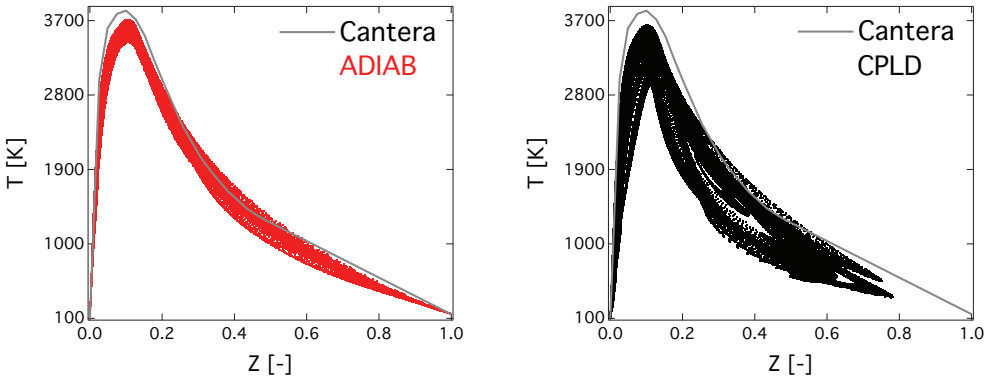

(a) Adiabatic Case (b) Coupled Case

Figure 8.13: Scatter plot of the Temperature vs. the mixture fraction in the splitter configuration. Box 2.

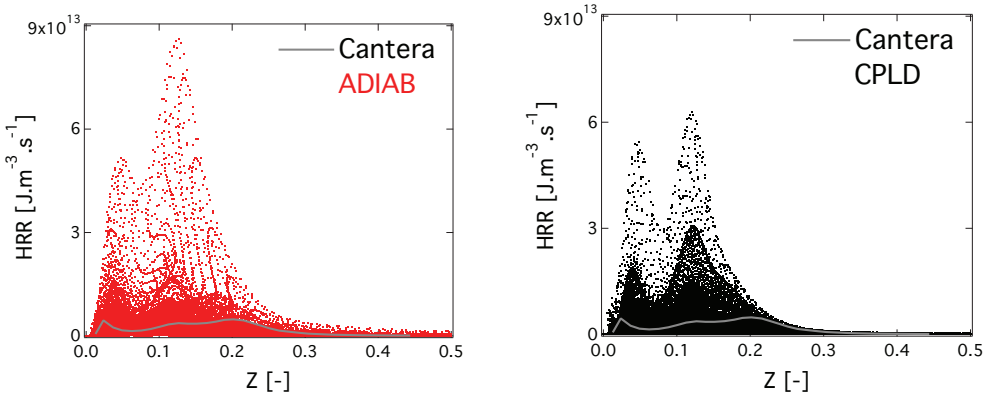

(a) Adiabatic Case (b) Coupled Case

Figure 8.14: Scatter plot of the Heat Release Rate vs. the mixture fraction in the splitter configuration. Box 2.

Box 2 corresponds to a region where turbulence is developed (Fig. 8.7). The flame is highly wrinkled and local extinction by turbulence is likely. Nevertheless, in both adiabatic and coupled cases the temperature scatter plot shows no points

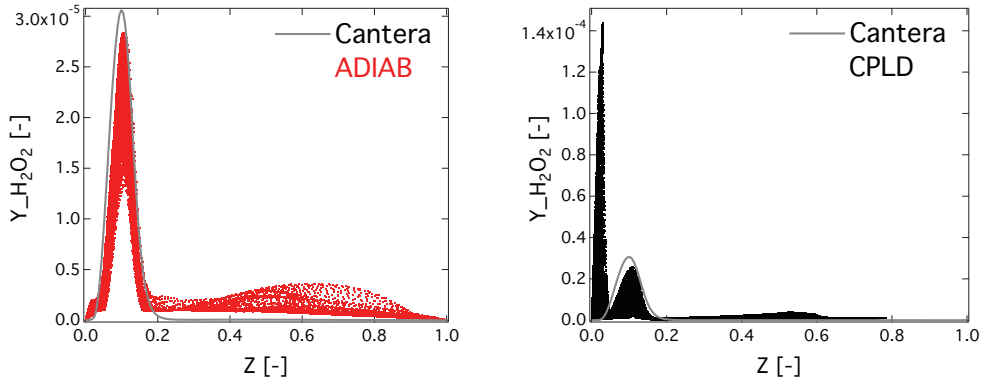

(a) Adiabatic Case (b) Coupled Case

Figure 8.15: Scatter plot of the H_2O_2 radical vs. the mixture fraction in the splitter configuration. Box 2.

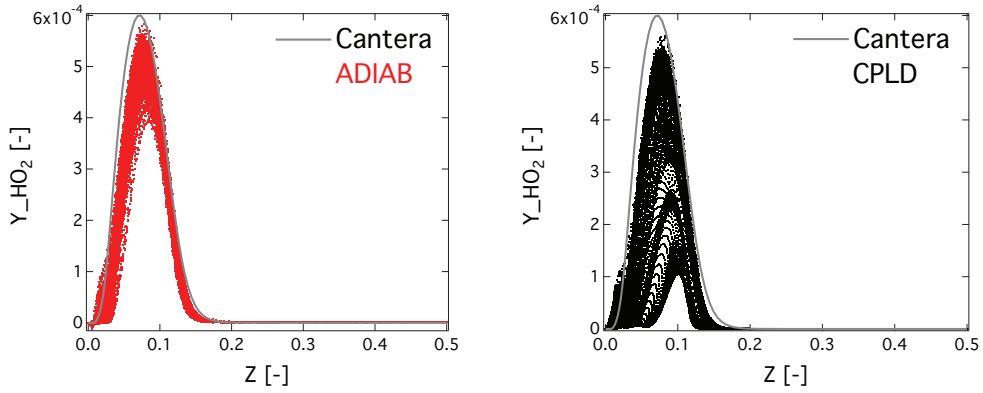

(a) Adiabatic Case (b) Coupled Case

Figure 8.16: Scatter plot of the HO_2 radical vs. the mixture fraction in the splitter configuration. Box 2.

on the mixing line. The heat release rate peaks at the stoichiometric value but the lean secondary peak is still visible. For both cases the maximum value of the heat release rate are comparable around $6\,10^{13}$ and $9\,10^{13}$ J.m^3.s^{-1}. Overall, in the adiabatic case, the flame structure is very similar to that in Box 1 but combustion is more intense, as revealed by the higher values of the heat release rate. As can be seen in Fig. 8.7, the turbulence increases the local strain rate leading to a collection of pure H_2/O_2 counterflow flames increasing the heat release rate.

As for the NEMO configuration, because of the heat loss at the wall the flame chemical structure is highly modified in the vicinity of the injector. Large

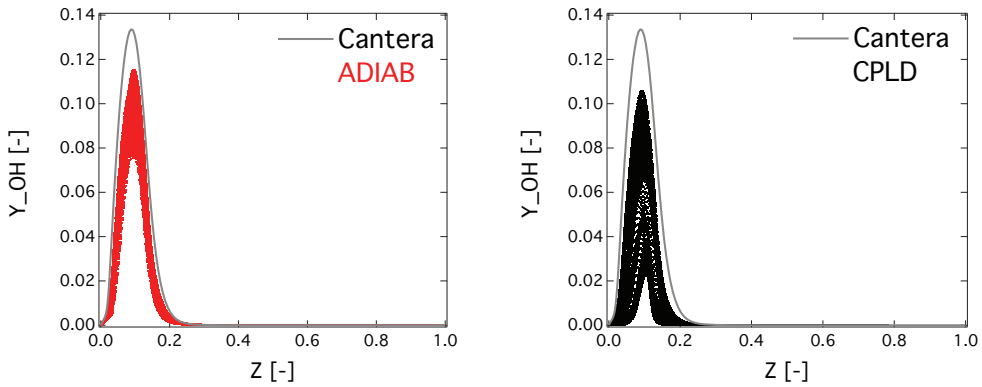

(a) Adiabatic Case (b) Coupled Case

Figure 8.17: Scatter plot of the OH radical vs. the mixture fraction in the splitter configuration. Box 2.

amounts of radicals, such as H_2O_2 or HO_2, are produced close to the wall. The next section will address the question of the impact of these modifications on the flame anchoring mechanisms.

8.5.2 Flame stabilization

Experimental OH fluorescence images obtained by [Singla 2006] in transcritical conditions. Because of the high density and low velocity of the LOx stream the configuration can be compared to a backward facing step as shown in Fig. 8.18. Previous studies as in [Juniper 2003b] have indicated that the flame edge is close to the injector lip, therefore in the near vicinity of the hydrogen stream.

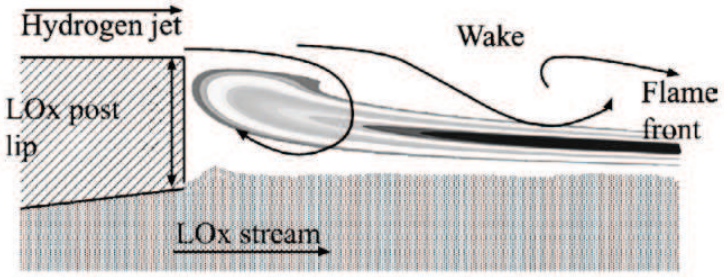

Figure 8.18: Schematic representation of the flame stabilized in the recirculation zone behind the injector. Extracted from [Singla 2006]

A detailed analysis of the flow indicates that the flame is anchored when its thickness is smaller than the transverse dimension of the wake established by the injector lip. An important parameter introduced is the characteristic ratio ψ defined as the ratio between the lip thickness e and a flame thickness δ_f

$$\psi = \frac{e}{\delta_f} \tag{8.22}$$

As the combustion occurs in a diffusion regime, the flame thickness can not be defined as in premixed configuration but it can be evaluated as

$$\delta_f = \sqrt{\tau_c \, D} \tag{8.23}$$

where τ_c is the characteristic chemical time and D the mass diffusivity of the burnt gases. The characteristic chemical time can be evaluated using the stoichiometric premixed laminar flame at the same thermodynamics conditions. It reads

$$\tau_c = \frac{\delta_l}{S_l^0} \tag{8.24}$$

Using results from Chap. 7 we obtain $\tau_c = 1.31\,10^{-7}$ s at 100 bar and 300 K. The mass diffusivity of the burnt gases (water) is evaluated using the constant Schmidt number approximation (Tab. 8.3) $D \sim 1\,10^{-8}$ m^2.s^{-1}. Finally the flame thickness in these thermodynamic conditions is $\delta_f \sim 10^{-6}$ m. This leads to a dimensionless lip height of $\psi \sim 10^{-4}/10^{-6} = 10^2$.
In [Juniper 2003b] the authors demonstrate that the flame is anchored when $\psi > 1$ and becomes unstable and sensitive to the high speed hydrogen flow when $\psi < 1$.

Thus in the present configuration the flame should be well anchored in the wake of the injector tip.

As shown in Fig. 8.19 for both wall boundary conditions non-zero heat release rate is found at the wall. However the phenomena in both cases are very different. In the adiabatic case the heat release rate exhibits three distinct branches. This structure has been identified in the strained counterflow diffusion flame configuration and is characteristic of the detailed chemistry used for the H_2/O_2 combustion. The heat release rate spreads almost over the entire thickness of the splitter. In the coupled case the heat release rate shape is very different. A very strong and thin heat release rate peaks at the bottom of the wall. This large production is due to reactions with low or zero activation energy enabled at the wall as it was shown in Chap. 7.

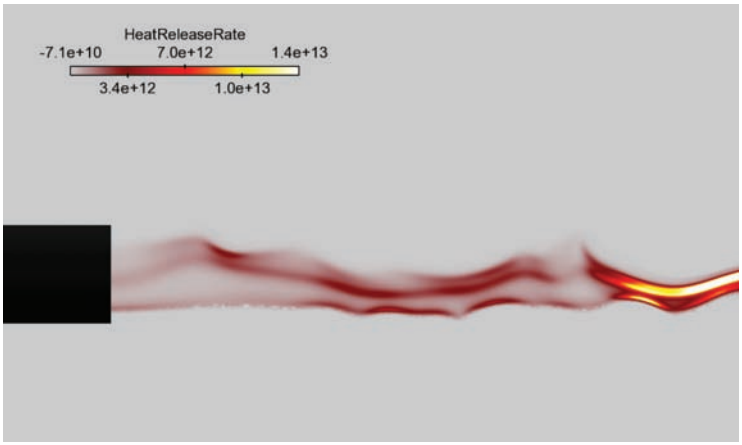

(a) Adiabatic Case

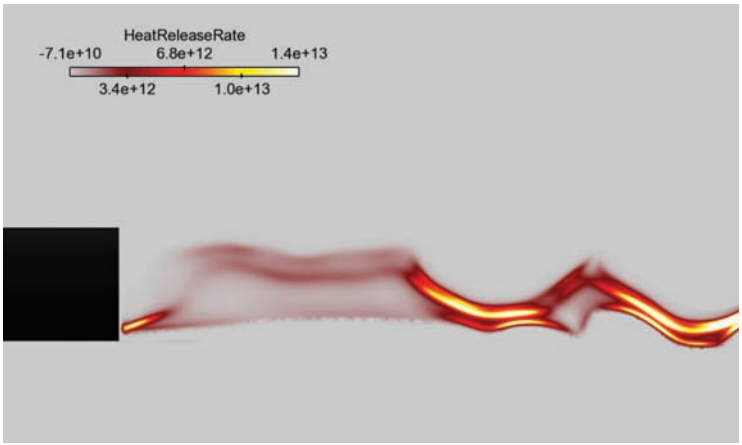

(b) Coupled Case

Figure 8.19: Instantaneous field of heat release rate in the splitter configuration.

Figure 8.20 shows an instantaneous field of the OH mass fraction in the near vicinity

of the injector tip for both boundary conditions and from experimental OH-PLIF. In the adiabatic case, OH radical is produced at the wall and the flame seems well anchored thanks to this radical.
In the coupled case, OH mass fraction is lifted from the injector at a short distance. The OH maximum stands at around one splitter thickness.
This phenomenon has been already highlighted in Chap. 7 and is due to the chemical reactions that delay the production of the OH radical where the influence of the low temperature wall has vanished. These reactions have a non-zero activation energy and are disabled by the low temperature of the wall in the coupled simulation.
This result is in good agreement with the experimental data of [Singla 2006] obtained at a pressure of $P = 6.3$ MPa with a splitter of 0.3 mm, using the OH-PLIF technique. They showed in Fig. 8.20(c) that the flame anchoring point, based on the OH emission, is lifted above the tip of the injector and is fluctuating with time. They concluded that the OH layer thickness, of the order of the lip thickness, indicates that the flame is sensitive to the high-speed hydrogen stream. In the coupled simulation the OH layer is smaller than in the experimental OH-PLIF image because of the higher pressure leading to a smaller flame thickness.
For a more quantitative comparison, Fig. 8.21 shows the position of the maximum of the OH mass fraction in the vicinity of the splitter at several instants. Results extracted from [Singla 2006] and from the coupled computation compares favorably. The OH maximum position fluctuates with time between one and two injector thickness.

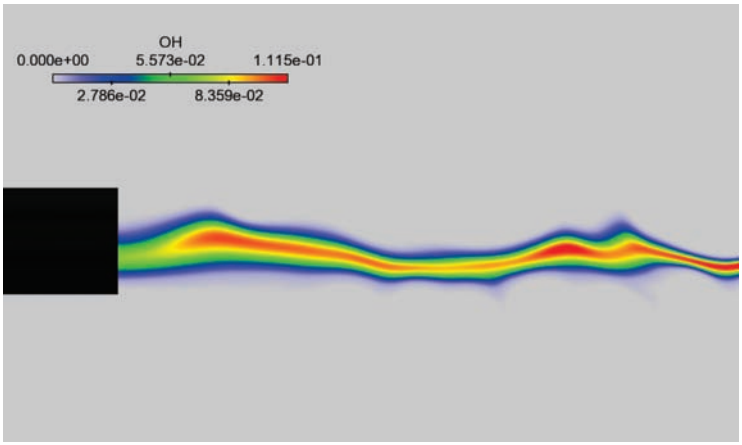

(a) Adiabatic Case

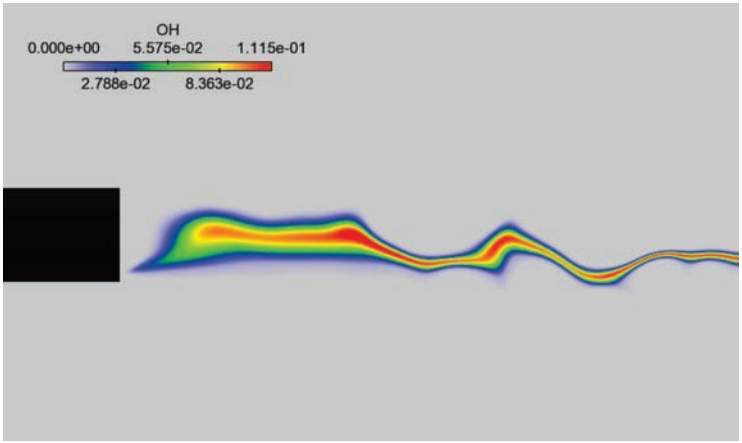

(b) Coupled Case

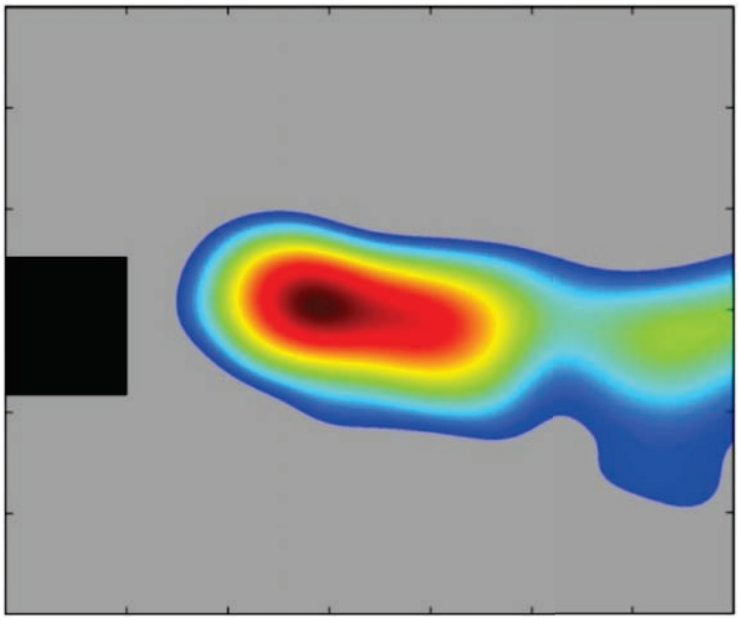

(c) OH-PLIF visualization of the near vicinity of the injector lip. Extracted from [Singla 2006].

Figure 8.20: Instantaneous field of the OH mass fraction in the splitter configuration. Liquid oxygen and gaseous hydrogen are injected below and above the step, respectively.

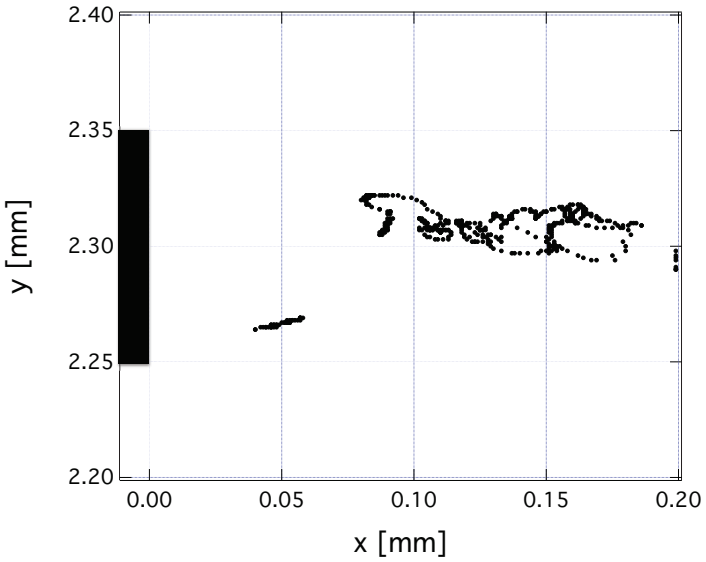

(a) Coupled LES. The injector is located from $y = 2.25$ mm and $y = 2.35$ mm (*black rectangle*).

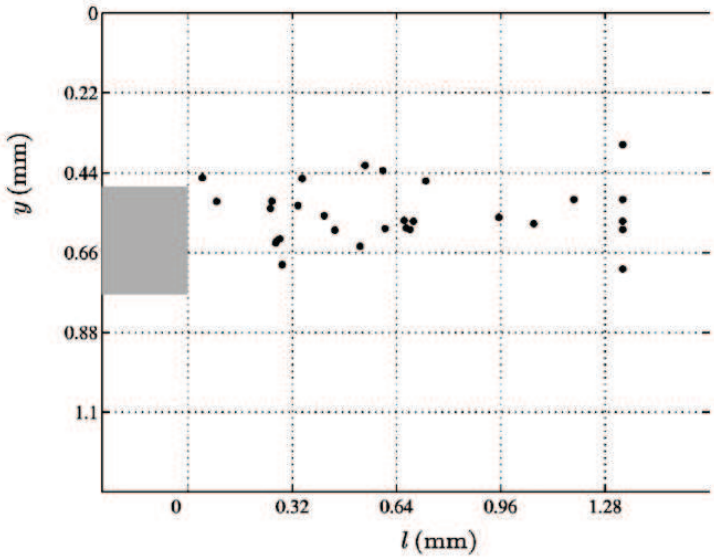

(b) OH-PLIF images. Extracted from [Singla 2006]

Figure 8.21: Position of the maximum OH mass fraction in the near vicinity of the injector at several instants for the splitter configuration.

In [Singla 2006] it was concluded that the flame sensitivity to the hydrogen high velocity stream could lead to a lift-off or even blow-off. However blow-off was never observed in the experiment, and the authors speculated that the flame probably anchors at some other circumferential locations.
Figure 8.22 and Fig. 8.23 compare the production rate of the H_2O_2 and HO_2 radicals in the wake of the injector for the adiabatic and coupled cases.
In the adiabatic case, both fields are comparable to the OH radical field shown in Fig. 8.20a. This may indicate that OH stays a good marker of the flame location. In the coupled case, H_2O_2 and HO_2 radicals build up at the wall, acting as flame precursors and initiating the chemical reactions chain. As shown for the 1D flame in Chap. 7, the mechanism of the flame anchoring at the wall is due to H_2O_2 and HO_2 radicals. The reactions producing these radicals (such as $R10$) have zero or low energy of activation and become dominant at the wall (Fig. 8.24). These mechanisms have been extensively developed in Chap. 7 and coupled simulations confirm that they remain valid in the present case.

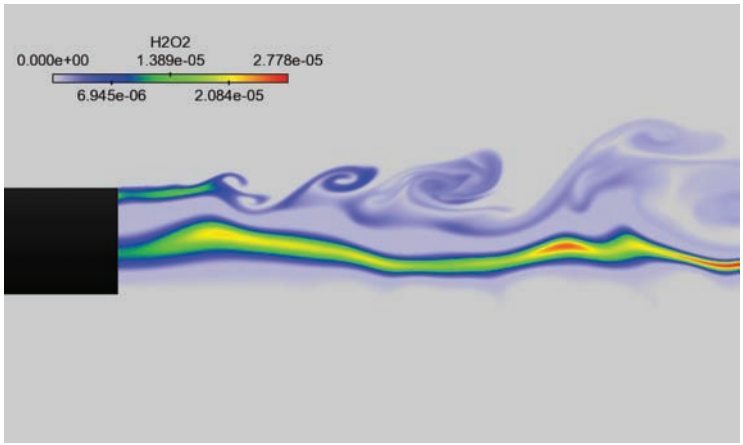

(a) Adiabatic Case

(b) Coupled Case

Figure 8.22: Instantaneous field of H_2O_2 mass fraction. For clarity reasons scaling maximum is 2.778 10^{-5} in the adiabatic case and 2 10^{-3} in the coupled case.

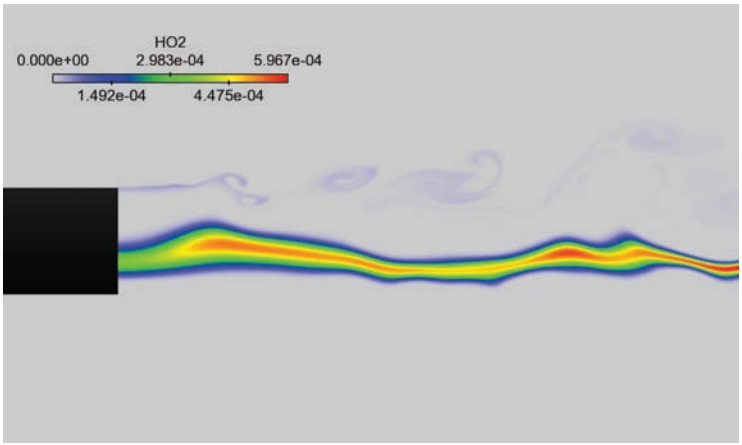

(a) Adiabatic Case

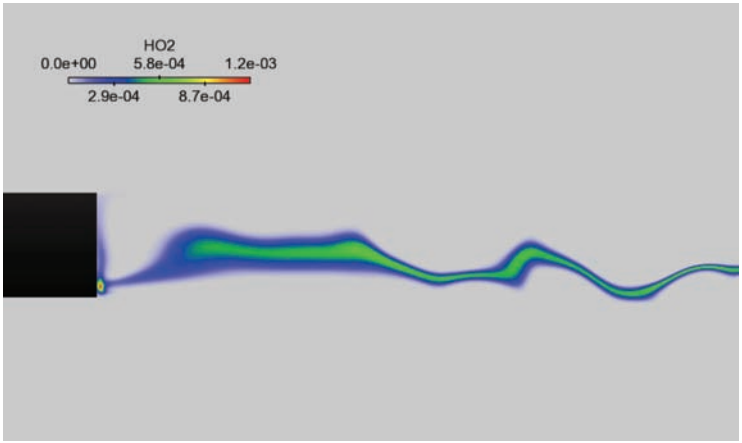

(b) Coupled Case

Figure 8.23: Instantaneous field of HO_2 mass fraction. For clarity reasons scaling maximum is 5.976 10^{-4} in the adiabatic case and 1.2 10^{-3} in the coupled case.

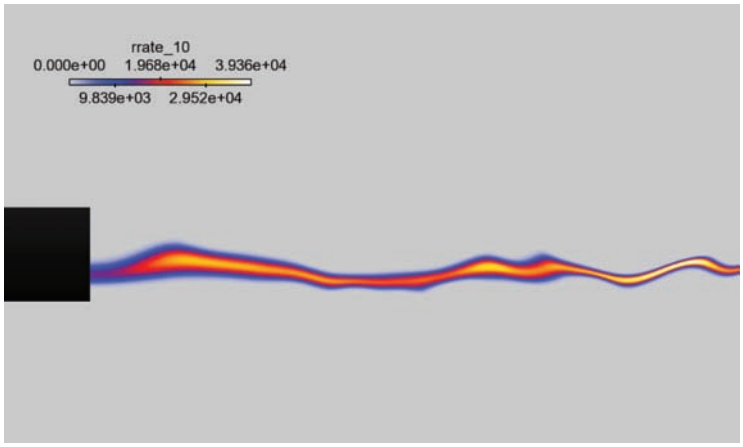

(a) Adiabatic Case

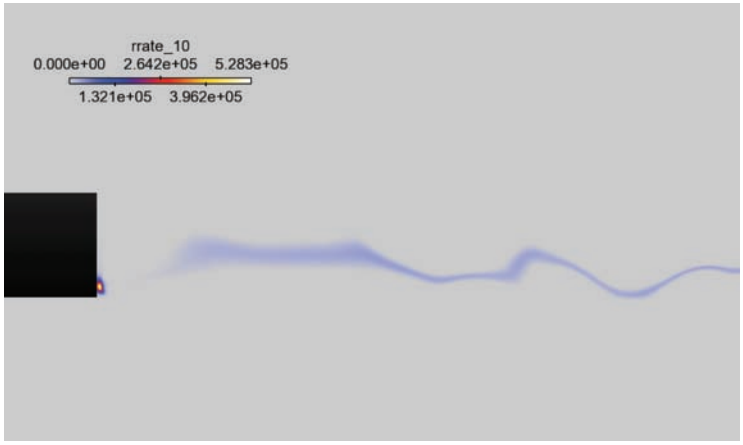

(b) Coupled Case

Figure 8.24: Instantaneous reaction rate of Reaction 10. For clarity reasons the scale maximum is 3.936 10^4 in the adiabatic case and 5.283 10^5 in the coupled case.

8.5.3 Temperature fields and thermal fluxes

Figure 8.25 and 8.25 show the temperature fields in the adiabatic and coupled cases (resp.). In the simulation using adiabatic boundary condition at the lip (Fig. 8.25) the thickness of the high temperature zone is of the order of the lip thickness. This is due to the zero-flux condition at the wall which allows the flame to develop right at the wall, almost as a simple strained diffusion flame. The detailed mechanisms and the flame structure has been examined in detail in the previous section.

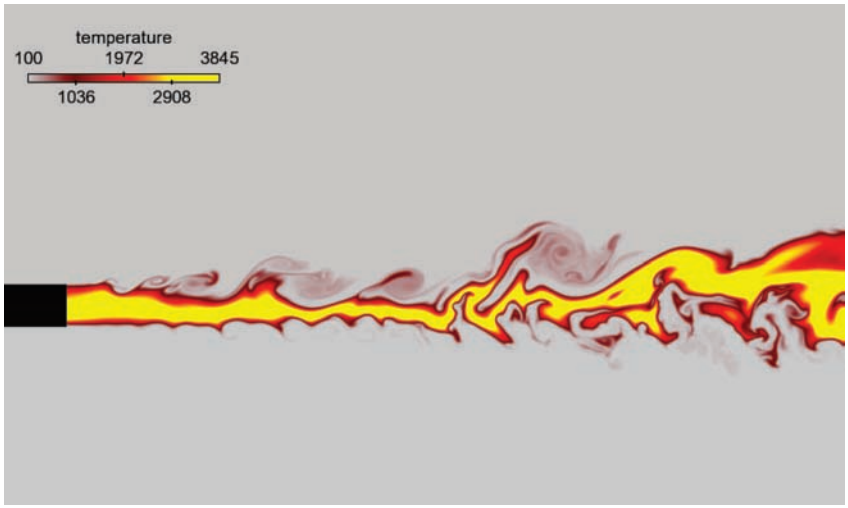

(a) Global view.

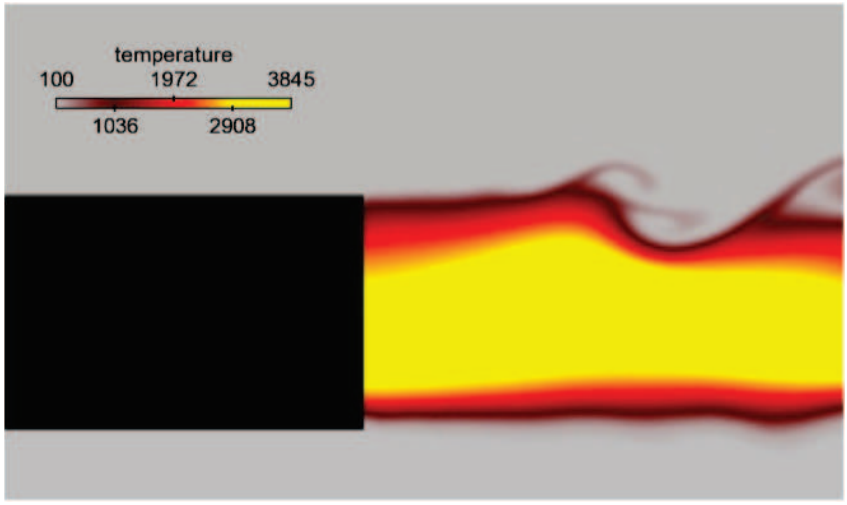

(b) Zoom on the lip region.

Figure 8.25: Instantaneous field of temperature. Adiabatic simulation.

In the coupled simulation, the heat transferred to the solid is maximum at the

bottom of the lip where the flame anchors as shown in Fig. 8.6. The maximum temperature in the solid reaches around 360 K as shown in Fig. 8.26, which is close to the value predicted by the previous theoretical study with the Neumann boundary condition ($T_p = 357$ K). It is located at the bottom of the lip but the solid temperature field rapidly becomes one-dimensional. The temperature penetration length is slightly higher than one injector thickness, which validates *a posteriori* the theoretical study and the injector length chosen for the computation.

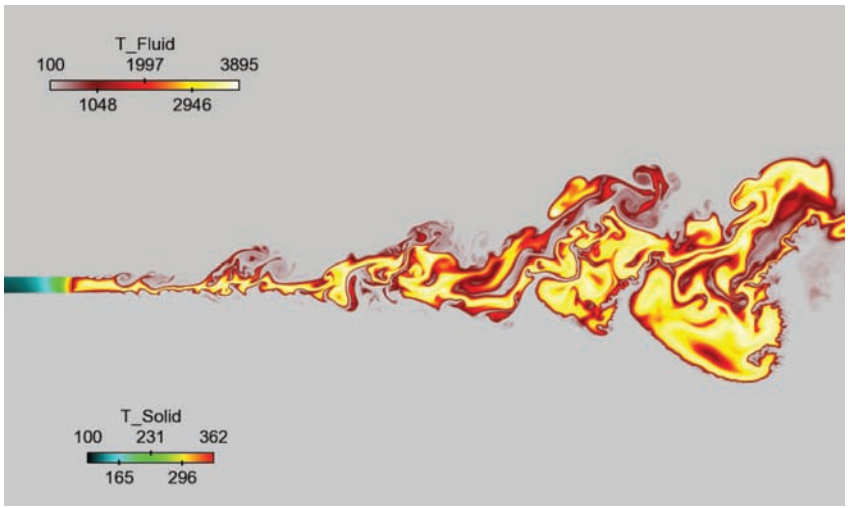

(a) Global view.

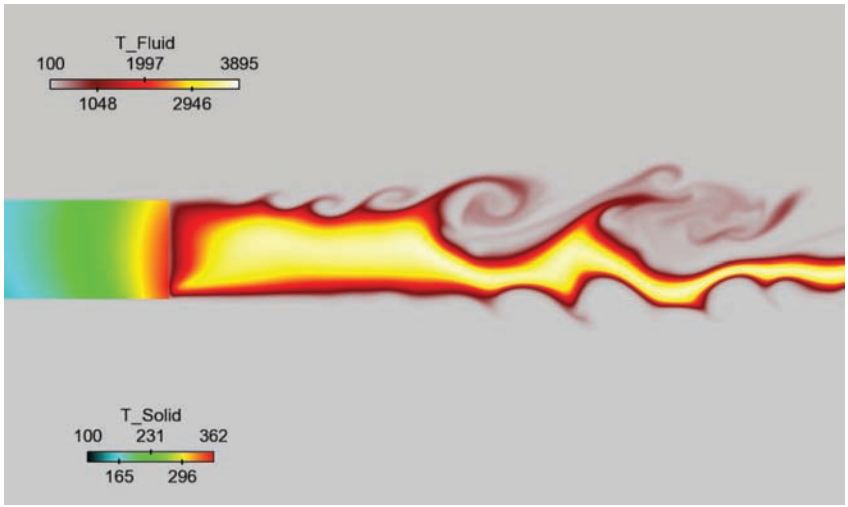

(b) Zoom on the lip region.

Figure 8.26: Instantaneous field of temperature. Coupled simulation of the splitter case.

The solid temperature field is zoomed in Fig. 8.27. It is almost one dimensional except very near to the bottom right corner. The thermal flux plotted in Fig. 8.27(b),

indicates that in the first half from the tip of the injector the flux is almost along the axial direction and comes from the front of the injector where the flame stands. In the second half of the splitter, the influence of the flame vanishes and the flux is almost transverse. Because of its higher temperature (150 K), the H_2 stream transfers some heat to the solid which then transfers it back to the oxygen stream.

(a) Temperature field in the solid.

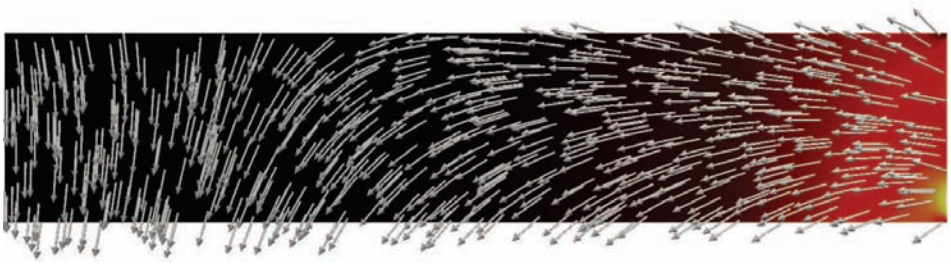

(b) Thermal flux. Arrows are not proportional to the flux value for the coupled simulation of the splitter.

Figure 8.27: Solid stationary thermal fields.

The time evolution of the thermal flux on a probe located on the front face of the splitter, at $1/5^{th}$ of the splitter height is plotted in Fig. 8.28. The probe is located close to the flame anchoring region. The flux peaks at a value of $\sim 5\,10^8$ W.m^2 at the beginning of the computation corresponding to the impact of the flame on the wall after the ignition. Then it stabilizes at $\sim 1\,10^8$ W.m^2 and remains almost constant with time.
This flux can now be used for thermal fatigue calculation of the injector. It is however a mean flux, and the same methodology could be repeated with a synchronous coupling strategy. This would allow to obtain the instantaneous, possibly intermittent flux. However it seems that the flame is very stable so that the mean heat flux may be sufficient.

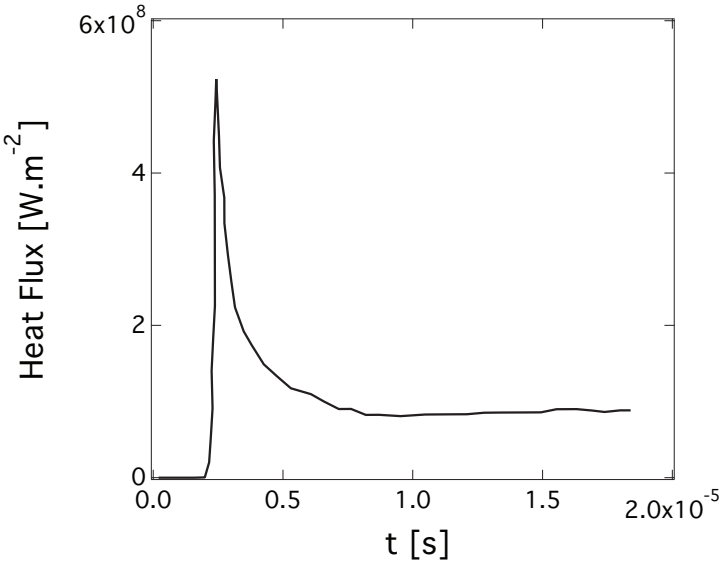

Figure 8.28: Time evolution of the heat flux on a probe located on the front face of the splitter close to the flame anchoring region.

Part IV

Conclusions and Perspectives

Chapter 9

Conclusion and Perspectives

Contents

The objective of this work was to study the the impact of the heat transfer on high pressure flames in Liquid Rocket Engine context. To achieve this goal a conjugate heat transfer methodology using a thermal solver coupled to a fluid solver was used.

The introduction of the manuscript is dedicated to the context, scientific and industrial, and a literature review is conducted in order to put this work in the actual scientific context. A special attention is payed to the thermodynamics of real gas. Several equations of state are compared in order to evaluate their accuracy/computational cost ratio. Modifications of the transport coefficient due to high pressure regime is also introduced. The coupling strategy along with the thermal solver and the requirements to ensure mass conservation are then exposed.
In the second part, the coupling strategy is then applied to a coaxial CH_4/O_2 atmospheric burner. This configuration was experimentally studied at EM2C by T. Schmitt and P. Scoufflaire. The burner is equipped with thermocouples along the internal tube in order to measure the temperature distribution. Several flow measurements, such as PIV, OH-PLIF and hot wire, were also done to characterize the flow field and the combustion.
A detailed chemical kinetic scheme was used in the LES to capture flame features. It was extensively validated on simple 1D configurations for both premixed and diffusive flames with CANTERA software.

The experimental results were compared to LES for two different regimes, laminar and turbulent, of the injector. In both cases, thermal distribution in the burner compares favorably validating the coupling methodology. Moreover, this study allowed to explore the chemical kinetic modification due to the heat loss at the wall. It was concluded that the low temperature at the wall enhances some radicals production while disabling high energy of activation reactions.
The third part presents the results of Direct Numerical Simulations of hydrogen / oxygen flames in supercritical conditions representative of a Liquid Rocket Engine.

The first section of the third part presents an article submitted to the journal *Combustion & Flame*. In a first time, the effects of fluid/solid coupling on Flame Wall Interaction were investigated. It was shown that if the effusivity of the burnt gases

becomes non-negligible compare to that of the solid, the isothermal assumption does not hold anymore justifying the coupled approach for LRE configurations. In the second part effects of pressure were studied up to 100 bar where real-gas effects appear. It allowed to exhibit the quenching phenomena and its impact on the flame structure. The importance of a detailed chemistry and the crucial role played by the radical such as HO_2 or H_2O_2 have been demonstrated.

Finally the last part was dedicated to the study of a 2D DNS under supercritical thermodynamic conditions, typical of a Liquid Rocket Engine. The coupling strategy developed in Chap. 4 has been applied and the structure of the flame was analyzed in the mixture fraction space. It is shown that partial premixing occurs, due to the high heat loss at the wall. The tip of the splitter plate is heated up by the burnt gases but the location of the flame anchoring and the downstream evolution of the flame are marginally affected. Finally the thermal fluxes and the temperature of the solid were investigated to later conduct thermal fatigue calculations.
To summarize, a methodology to compute heat transfer, coupled with LES of real-gas, turbulent reacting flows has been developed, validated and applied to a configuration representative of Liquid Rocket Engines. Results show the impact on the combustor behavior and and the importance of introducing the heat exchanges between the fluid and the solid. The methodology can now be applied to other configurations such as full combustion chambers to study cooling techniques for example.

Perspectives Several improvements can be considered:

- all the simulations done in this work use no-slip walls and require a good resolution of the viscous sub-layer ($y^+ < 5$) in order to capture the wall heat exchange coefficient. Unfortunately, in most LES such refinement at the wall is incompatible with computation time and CPU cost. Thus this coupling strategy could be extended to wall law with or without chemical reaction.

- during the coupled simulations done in this work all walls were considered chemically inert. This hypothesis has not been confirmed and should be verified to eventually take into account wall kinetic reactions.

- radiative effects have also been neglected and could be investigated using the PRISSMA code, coupled with the AVBP-AVTP framework used in this work.

During the thesis, the developed methodology was also applied to an industrial configuration, not presented here for confidentiality reasons. The predictive capabilities in terms of thermal fluxes were confirmed and the feasibility of fully coupled aerospace combustion chamber using LES was demonstrated. Such simulations are now run in the industrial environment at Snecma.

Bibliography

[Amaya 2010a] J. Amaya. *Unsteady coupled convection, conduction and radiation simulations on parallel architectures for combustion applications.* PhD thesis, INP Toulouse, 2010. (Cited on page 67.)

[Amaya 2010b] J. Amaya, O. Cabrit, D. Poitou, B. Cuenot and M. El Hafi. *Unsteady coupling of Navier-Stokes and radiative heat transfer solvers applied to an anisothermal multicomponent turbulent channel flow.* , vol. 111, no. 2, pages 295–301, January 2010. (Cited on pages 58 and 67.)

[Assembly 2008] United Nations General Assembly. *Report of the United Nations/Russian Federation/European Space Agency workshop on the use of Microsatellite Technologies for monitoring the environment and its impact on human health.* United Nations, 2008. (Cited on page 6.)

[Baum 1995] M. Baum, T. Poinsot and D. Thévenin. *Accurate Boundary Conditions for Multicomponent Reactive Flows.* Journal of Computational Physics, vol. 116, no. 2, pages 247–261, 1995. (Cited on page 199.)

[Bellan 2000] J. Bellan. *Supercritical (and subcritical) fluid behavior and modeling: drops, streams, shear and mixing layers, jets and sprays.* Progress in Energy and Combustion Science, vol. 26, pages 329–366, 2000. (Cited on pages 12, 17, 41 and 197.)

[Bellan 2006] J. Bellan. *Theory, modeling and analysis of turbulent supercritical mixing.* Combust. Sci. Tech. , vol. 178, pages 253–281, 2006. (Cited on page 19.)

[Bilger 1990] R. W. Bilger, B. Yip, M. B. Long and A. R. Masri. *An atlas of QEDR flame structures.* Combust. Sci. Tech. , vol. 72, no. 4-6, pages 137–155, 1990. (Cited on page 133.)

[Bird 1960] R. B. Bird, W. E. Stewart and E. N. Lighfoot. Transport phenomena. John Wiley, New York, 1960. (Cited on page 53.)

[Bogey 2011] Christophe Bogey, Olivier Marsden and Christophe Bailly. *Large-eddy simulation of the flow and acoustic fields of a Reynolds number 10[sup 5] subsonic jet with tripped exit boundary layers.* Physics of Fluids, vol. 23, no. 3, page 035104, 2011. (Cited on page 199.)

[Boivin 2011] P. Boivin, C. Jiménez, A.L. Sanchez and F. Williams. *An explicit reduced mechanism for H2–air combustion.* Proceedings of the Combustion Institute, vol. 33, no. 1, pages 517–523, 2011. (Cited on pages xvii, 164, 166 and 196.)

[Bowman 1998] C.T. Bowman, R.K. Hanson, W.C. Gardiner, V. Lissianki, M. Frenklach, M. Goldenberg and G.P Smith. *GRI-Mech 2.11: an optimized detailed chemical reaction mechanism for methane combustion and NO formation and reburning.* Gri-tech, Gas Research Institute, 1998. (Cited on page 78.)

[Branam 2003] R. Branam and W. Mayer. *Characterisation of Cryogenic Injection at Supercritical pressure.* J. Prop. Power , vol. 19, no. 3, pages 342–355, May-June 2003. (Cited on page 12.)

[Briones 2006] Alejandro M. Briones, Suresh K. Aggarwal and Viswanath R. Katta. *A numerical investigation of flame liftoff, stabilization, and blowout.* Physics of Fluids, vol. 18, no. 4, page 043603, 2006. (Cited on page 196.)

[Cabra 2002] R Cabra, T Myhrvold, JY Chen, RW Dibble, AN Karpetis and RS Barlow. *Simultaneous laser Raman-Rayleigh-LIF measurements and numerical modeling results of a lifted turbulent H2/N2 jet flame in a vitiated coflow.* Proceedings of the Combustion Institute, vol. 29, no. 2, pages 1881–1888, 2002. (Cited on page 196.)

[Cabrit 2009] O. Cabrit. *Modelisation des flux parietaux sur les tuyeres des moteurs a propergol solide.* PhD thesis, Universit/'e de Montpellier II, 2009. (Cited on page 149.)

[Candel 2006] S. Candel, M. Juniper, G. Singla, P. Scouflaire and C. Rolon. *Structure and Dynamics of Cryogenic Flames At Supercritical Pressure.* Combustion Science and Technology, vol. 178, no. 1-3, pages 161–192, January 2006. (Cited on pages ix, 16, 17 and 197.)

[Candel 2011] S. Candel, T. Schmitt and N. Darabiha. *Progress in transcritical combustion : experimentation, modeling and simulation.* In 23rd ICDERS. Irvine, USA, 2011. (Cited on pages ix and 15.)

[Chehroudi 2002] B. Chehroudi, D. Talley and E. Coy. *Visual characteristics and initial growth rate of round cryogenic jets at subcritical and supercritical pressures.* Phys. Fluids , vol. 14, no. 2, pages 850–861, 2002. (Cited on pages ix, 12, 14 and 19.)

[Chehroudi 2004] B. Chehroudi and D. Talley. *Fractal geometry of a cryogenic nitrogen round jet injected into sub- and super-critical conditions.* Atomization and Sprays, vol. 14, pages 81–91, 2004. (Cited on page 12.)

[Chen 1991] J.Y. Chen and R.W. Dibble. *Applications of reduced chemical mechanisms for the prediction of turbulent non premixed methane jet flames.* In M.D. Smooke, editeur, Reduced Kinetic Mechanisms and Asymptotic Approximations for Methane-Air Flames, volume 384, pages 193–226. Springer Verlag, 1991. (Cited on page 80.)

[Chen 1997] J.Y. Chen. *Development of reduced mechanisms for numerical modelling of turbulent combustion.* Workshop on numerical aspects of reduction in chemical kinetics. CERMICS-ENPC. Champus-sur-Marne, France, 1997. (Cited on page 79.)

[Chnafa 2010] C. Chnafa, G. Sonet, I. Laumond, C. Castagnie and F. Reynal. Characteristics of supercritical states - an experimental study. Lacapelle Science Publications, Aug. 2009-2010. (Not cited.)

[Chung 1984] T. H. Chung, L. L. Lee and K. E. Starling. *Applications of Kinetic Gas Theories and Multiparameter Correlation for Prediction of Dilute Gas Viscosity and Thermal Conductivity.* Industrial & Engineering Chemistry Fundamentals, vol. 23, pages 8–13, 1984. (Cited on pages 52 and 200.)

[Chung 1988] S. H. Chung and C. K. Law. *An integral analysis of the structure and propagation of premixed flames.* Combust. Flame , vol. 72, pages 325–336, 1988. (Cited on page 52.)

[Clifford 2002] T. Clifford. Fundamentals of supercritical fluids. Oxford Science Publications, 2002. (Cited on page 39.)

[CNES 2015] CNES, March 2015. (Cited on page 7.)

[Colin 2000] O. Colin, F. Ducros, D. Veynante and T. Poinsot. *A thickened flame model for large eddy simulations of turbulent premixed combustion.* Phys. Fluids , vol. 12, no. 7, pages 1843–1863, 2000. (Cited on page 112.)

[Congiunty 2003] A. Congiunty, C. Bruno and E. Giacomazzi. *Supercritical combustion properties.* In 41st ASME, Reno, NV, January 2003. (Cited on page 52.)

[Dittus 1930] F.W. Dittus and L.M.K. Boelter. *Heat transfer in automobile radiator of the tubular type.* University of California Publications in Engineering, 1930. (Cited on page 204.)

[Duchaine 2009a] F. Duchaine, A. Corpron, L. Pons, V. Moureau, F. Nicoud and T. Poinsot. *Development and assessment of a coupled strategy for conjugate heat transfer with Large Eddy Simulation: Application to a cooled turbine blade.* International Journal of Heat and Fluid Flow, vol. 30, no. 6, pages 1129–1141, December 2009. (Cited on page 209.)

[Duchaine 2009b] F. Duchaine, T. Morel and L.Y.M. Gicquel. *Computational-Fluid-Dynamics-Based Kriging Optimization Tool for Aeronautical Combustion Chambers.* AIAA Journal, vol. 47, no. 3, pages 631–645, 2009. (Cited on page 66.)

[Duchaine 2013] F. Duchaine, N. Maheu, V. Moureau, G. Balarac and S. Moreau. *Large-Eddy Simulation and Conjugate Heat Transfer Around a Low-Mach Turbine Blade.* Journal of Turbomachinery, vol. 136, no. 5, 2013. (Cited on pages 58, 61 and 62.)

[Ely 1981a] J. F. Ely and H. J. M. Hanley. *Predictions of Transport Properties. 1. Viscosity of Fluids and Mixtures.* Industrial and Engineering Chemistry Fundamentals, vol. 20, no. 4, pages 323–332, 1981. (Cited on page 52.)

[Ely 1981b] J. F. Ely and H. J. M. Hanley. *Predictions of Transport Properties. 2. Thermal Conductivity of Pure Fluids and Mixtures.* Industrial and Engineering Chemistry Fundamentals, vol. 22, no. 4, pages 90–97, 1981. (Cited on page 52.)

[Ely 1992] J. F. Ely and M. L. Huber. Nist thermophysical properties of hydrocarbon mixtures. Gaithersburg, Maryland, July 1992. (Cited on page 47.)

[Esnault-Pelterie 1913] R. Esnault-Pelterie. *Considerations sur les resultats d'un allegement indefini des moteurs.* Journal de physique theorique et appliquee, 1913. (Cited on page 3.)

[Ezekoye 1992] O. A. Ezekoye, R. Greif and D. Lee. *Increased surface temperature effects on wall heat transfer during unsteady flame quenching.* In 24th Symp. (Int.) on Combustion, pages 1465–1472. The Combustion Institute, Pittsburgh, 1992. (Cited on page 164.)

[Favre-Marinet 2001] M. Favre-Marinet and EB Camano Schettini. *The density field of coaxial jets with large velocity ratio and large density differences.* International journal of heat and mass transfer, vol. 44, no. 10, pages 1913–1924, 2001. (Cited on page 113.)

[Franzelli 2010] B. Franzelli, E. Riber, M. Sanjosé and T. Poinsot. *A two-step chemical scheme for Large-Eddy Simulation of kerosene-air flames.* Combust. Flame , vol. 157, no. 7, pages 1364–1373, 2010. (Cited on pages 79 and 80.)

[Franzelli 2011] B. Franzelli. *Impact of the chemical description on direct numerical simulationsand large eddy simulations of turbulent combustion in industrial aero-engines.* PhD thesis, INP Toulouse, CERFACS - CFD Team, Toulouse, September 2011. (Cited on pages 80 and 105.)

[Frassoldati 2009] A Frassoldati, A Cuoci, T Faravelli, E Ranzi, C Candusso and D Tolazzi. *Simplified kinetic schemes for oxy-fuel combustion.* In 1st International Conference on Sustainable Fossil Fuels for Future Energy, pages 6–10, 2009. (Cited on pages 79 and 84.)

[Fraysse 2008] V. Fraysse, L. Giraud and S. Gratton. *A Set of Flexible GMRES Routines for Real and Complex Arithmetics on High-Performance Computers.* ACM Transactions on Mathematical Software, vol. 35, no. 2, 2008. (Cited on page 68.)

[Frenklach 1995] M. Frenklach, H. Wang, M. Goldenberg, G. P. Smith, D. M. Golden, C. T. Bowman, R. K. Hanson, W. C. Gardiner and V. Lissianki. *GRI-Mech: an optimized detailed chemical reaction mechanism for methane*

combustion. Rapport technique GRI-Report GRI-95/0058, Gas Research Institute, 1995. (Cited on page 78.)

[Gallois 2014] D. Gallois. *Ariane 6: Accord historique des européens*. Le Monde, vol. Economie & Entreprise, pages 1,3, December, 3rd 2014. (Cited on page 7.)

[Gilbert 1983] R. G. Gilbert, K. Luther and J. Troe. *Theory of Thermal Unimolecular Reactions in the Fall-off Range*. Ber. Bunsenges. Phys. Chem., vol. 87, page 169:177, 1983. (Cited on page 165.)

[Giles 1997] M.B. Giles. *Stability analysis of numerical interface conditions in fluid-structure thermal analysis*. Int. J. Numer. Meth. Fluids , vol. 25, no. 4, pages 421–436, 1997. (Cited on page 61.)

[Giovangigli 2011] V. Giovangigli, L. Matuszewski and F. Dupoirieux. *Detailed modeling of planar transcritical H2-O2-N2 flames*. Combustion Theory and Modelling, vol. 15, no. 2, pages 141–182, 2011. (Cited on pages 19, 197 and 200.)

[Goddard 1919] R. Goddard. A method of reaching extreme altitudes, volume 71 of *Smithsonian Miscallaneous Collections*. City of Washington, Smithsonian Institution, 1919. (Cited on page 3.)

[Goodwin 2009] D. G. Goodwin. *Cantera : An object-oriented software toolkit for chemical kinetics, thermodynamics, and transport processes*, July 2009. (Cited on page 80.)

[Habiballah 1996] M. Habiballah, L. Vingert, JC Traineau and P. Vuillermoz. *MASCOTTE- A test bench for cryogenic combustion research*. In IAF, International Astronautical Congress, 47 th, Beijing, China, 1996. (Cited on page 14.)

[Hirschfelder 1954] J. Hirschfelder, C. Curtis and B. Bird. Molecular theory of gases and liquids. John Wiley & Sons, 1954 edition, 1954. (Cited on pages x, 42, 44 and 53.)

[Hunt 1988] J. C. R. Hunt, A. A. Wray and P. Moin. *Eddies, streams, and convergence zones in turbulent flows*. In Proc. of the Summer Program , pages 193–208. Center for Turbulence Research, NASA Ames/Stanford Univ., 1988. (Cited on page 114.)

[Hussain 1995] F. Hussain and J. Jeong. *On the identification of a vortex*. J. Fluid Mech. , vol. 285, pages 69–94, 1995. (Cited on page 114.)

[Jacobsen 1973] R. T. Jacobsen and R. B. Stewart. *Thermodynamic Properties of Nitrogen Including Liquid and Vapor Phases from 63K to 2000K with Pressure to 10,000 bar*. Journal of Physical and Chemical Reference Data, vol. 2, no. 4, pages 757–922, 1973. (Cited on page 46.)

[Jauré 2011] S. Jauré, F. Duchaine and L. Gicquel. *Comparisons of Coupling Strategies for Massively Parallel Conjugate Heat Transfer with Large Eddy Simulation.* In In IV International Conference on Computational Methods for Coupled Problems in Science and Engineering, Kos Island, Greece, 2011. (Cited on page 58.)

[Jauré 2012] S. Jauré. *Methodology for conjugate heat transfer simulations relying on Large Eddy Simulations in massively parallel environments.* PhD thesis, INP Toulouse, 2012. (Cited on page 67.)

[Jauré 2013] S. Jauré, F. Duchaine, G. Staffelbach and L.Y.M. Gicquel. *Massively parallel conjugate heat transfer methods relying on large eddy simulation applied to an aeronautical combustor.* Computational Science & Discovery, vol. 6, no. 1, 2013. (Cited on pages 61 and 63.)

[Jones 1988] W. P. Jones and R. P. Lindstedt. *Global Reaction Schemes for Hydrocarbon Combustion.* Combust. Flame , vol. 73, pages 222–233, 1988. (Cited on page 79.)

[Juniper 2000] M. Juniper, A. Tripathi, P. Scouflaire, JC Rolon and S. Candel. *Structure of cryogenic flames at elevated pressures.* Proc. Combust. Inst. , vol. 28, no. 1, pages 1103–1110, 2000. (Cited on page 20.)

[Juniper 2001] M. Juniper, B. Leroux, F. Lacas and S. Candel. Stabilization of cryogenic flames and effect of recess, pages 221–231. Cepadues, 2001. (Cited on pages ix, 16 and 207.)

[Juniper 2003a] M. Juniper and S. Candel. *Stabilization of an edge diffusion flame behind a step over a liquid reactant.* J. Prop. Power , vol. 19, pages 332–342, 2003. (Cited on pages ix, 20 and 21.)

[Juniper 2003b] Matthew Juniper and Sébastien Candel. *Edge diffusion flame stabilization behind a step over a liquid reactant.* Journal of propulsion and power, vol. 19, no. 3, pages 332–341, 2003. (Cited on pages 197 and 217.)

[Juniper 2003c] Matthew Juniper, Nasser Darabiha and Sébastien Candel. *The extinction limits of a hydrogen counterflow diffusion flame above liquid oxygen.* Combustion and flame, vol. 135, pages 87–96, 2003. (Cited on pages ix, 17, 18 and 19.)

[Kim 2011] T. Kim, Y. Kim and S.K. Kim. *Numerical analysis of gaseous hydrogen/liquid oxygen flamelet at supercritical pressures.* International Journal of Hydrogen Energy, 2011. (Cited on page 19.)

[Lacaze 2012] G. Lacaze and J.C. Oefelein. *A non-premixed combustion model based on flame structure analysis at supercritical pressures.* Combustion and Flame, 2012. (Cited on pages ix and 19.)

[Lamarque 2007] N. Lamarque. *Schémas numériques et conditions limites pour la simulation aux grandes échelles de la combustion diphasique dans les foyers d'hélicoptère*. Phd thesis, INP Toulouse, 2007. (Cited on pages 68 and 69.)

[Lasheras 1998] J.C. Lasheras, E. Villermaux and E. J. Hopfinger. *Break-up and atomization of a round water jet by a high-speed annular air jet*. J. Fluid Mech. , vol. 357, pages 351–379, 1998. (Cited on pages 14 and 113.)

[Lemmon 2007] E.W. Lemmon, M.L. Huber and M.O. McLinden. *NIST Standard Reference Database 23: Reference Fluid Thermodynamic and Transport Properties-REFPROP, Version 8.0*. Rapport technique, National Institute of Standards and Technology, Standard Reference Data Program: Gaithersburg, MD, 2007. (Cited on pages x, 50, 52, 54, 55 and 56.)

[Lemmon 2009] EW Lemmon, MO McLinden and DG Friend. *Thermophysical properties of fluid systems*. NIST chemistry webbook, NIST standard reference database, vol. 69, 2009. (Cited on pages xvii and 204.)

[Lindsey 2012] C. Lindsey. *DARPA developing microsat constellation orbited with air-launch system*. NewSpace Watch, 2012. (Cited on page 6.)

[Lodato 2008] Guido Lodato, Pascale Domingo and Luc Vervisch. *Three-dimensional boundary conditions for direct and large-eddy simulation of compressible viscous flows*. Journal of Computational Physics, vol. 227, no. 10, pages 5105–5143, May 2008. (Cited on page 199.)

[Lu 2008] T.F. Lu and C.K. Law. *A criterion based on computational singular perturbation for the identification of quasi-steady state species : A reduced mechanism for methane oxidation with NO chemistry*. Combustion and Flame, vol. 154, no. 4, pages 761–774, 2008. (Cited on pages 80, 84 and 160.)

[Lyons 2007] Kevin M. Lyons. *Toward an understanding of the stabilization mechanisms of lifted turbulent jet flames: Experiments*. Progress in Energy and Combustion Science, vol. 33, no. 2, pages 211–231, April 2007. (Cited on page 196.)

[Mari 2012] R. Mari, B. Cuenot, F. Duchaine and L. Selle. *Stabilization mechanisms of a supercritical hydrogen/oxygen flame*. In Proceedings of the 2012 Summer Program, pages 439–448. Center for Turbulence Research, NASA Ames/Stanford Univ., 2012. (Cited on page 212.)

[Masquelet 2009] M. Masquelet, S. Menon, Y. Jin and R. Friedrich. *Simulation of unsteady combustion in a LOX-GH2 fueled rocket engine*. Aerospace Science and Technology, 2009. (Cited on page 19.)

[Masquelet 2013] M. Masquelet. *Large Eddy Simulations of high-pressure shear coaxial flows relevant for H2/O2 rocket engines*. PhD thesis, Georgia Institute of Technology, 2013. (Cited on pages ix and 11.)

[Mayer 1996] W. Mayer and H. Tamura. *Propellant injection in a liquid oxygen/gaseous hydrogen rocket engine.* J. Prop. Power , vol. 12, no. 6, pages 1137–1147, November-December 1996. (Cited on page 14.)

[Mayer 1998] W.O.H. Mayer, R. Branan, D.G. Talley and R.D. Woodward. *Atomization and breakup of cryogenic propellants under high-pressure subcritical and supercritical conditions.* jpp, vol. 14, no. 5, pages 835–842, 1998. (Cited on page 12.)

[Mayer 2003] W. Mayer, J. Telaar, R. Branam, G. Schneider and J. Hussong. *Raman Measurements of Cryogenic Injection at Supercritical Pressure.* Heat and Mass Transfer, vol. 39, no. 8-9, pages 709–719, September 2003. (Cited on pages ix, 12, 13, 14 and 19.)

[Mayer 2004] W.O.H. Mayer and R. Branan. *Atomization characteristics on the surface of a round liquid jet.* Exp. Fluids , vol. 36, pages 528–539, 2004. (Cited on page 12.)

[Meng 2003] Hua Meng and Vigor Yang. *A Unified Treatment of General Fluid Thermodynamics and Its Application to a Preconditioning Scheme.* J. Comput. Phys. , vol. 189, pages 277–304, July 2003. (Cited on pages 33 and 197.)

[Miller 2001] Richard S. Miller, Kenneth G. Harstad and Josette Bellan. *Direct numerical simulations of supercritical fluid mixing layers applied to heptane-nitrogen.* Journal of Fluid Mechanics, vol. 436, pages 1–39, June 2001. (Cited on page 17.)

[Najm 1997] Habib N Najm and Peter S Wyckoff. *Premixed flame response to unsteady strain rate and curvature.* Combustion and Flame, vol. 110, no. 1, pages 92–112, 1997. (Cited on pages 79 and 84.)

[Nicoud 1999] F. Nicoud and F. Ducros. *Subgrid-scale stress modelling based on the square of the velocity gradient.* Flow, Turb. and Combustion , vol. 62, no. 3, pages 183–200, 1999. (Cited on pages 36 and 149.)

[Nikbay 2009] M. Nikbay, L. Öncü and A. Aysan. *Multidisciplinary Code Coupling for Analysis and Optimization of Aeroelastic Systems.* Journal of Aircraft, vol. 46, no. 6, pages 1938–1944, 2009. (Cited on page 58.)

[Nordsletten 2011] D.A. Nordsletten, S.A. Niederer, M.P. Nash, P.J. Hunter and N.P. Smith. *Coupling multi-physics models to cardiac mechanics.* Progress in Biophysics and Molecular Biology, vol. 104, pages 77–88, 2011. (Cited on page 58.)

[Oefelein 1997] J. C. Oefelein. *Simulation and analysis of turbulent multiphase combustion processes at high pressures.* PhD thesis, Pennsylvania State University, 1997. (Cited on pages ix, 19 and 20.)

[Oefelein 1998] Joseph C. Oefelein and Vigor Yang. *Modeling High-Pressure Mixing and Combustion Processes in Liquid Rocket Engines.* Journal of Propulsion and Power, vol. 14, no. 5, pages 843–857, September 1998. (Cited on page 197.)

[Oefelein 2005] J.C. Oefelein. *Thermophysical characteristics of shear-coaxial LOX-H2 flames at supercritical pressure.* Proceedings of the Combustion Institute, vol. 30, no. 2, pages 2929–2937, 2005. (Cited on pages 19 and 197.)

[Oefelein 2006] J. Oefelein. *Mixing and combustion of cryogenic oxygen-hydrogen shear-coaxial jet flames at supercritical pressure.* Combust. Sci. Tech. , vol. 178, no. 1-3, pages 229–252, 2006. (Cited on pages 19, 33 and 53.)

[Okong'o 2002a] N. Okong'o, K. Harstad and J. Bellan. *Direct numerical simulations of O2/H2 temporal mixing layers under supercritical conditions.* AIAA Journal , vol. 40, no. 5, pages 914–926, 2002. (Cited on pages 17 and 197.)

[Okong'O 2002b] Nora a. Okong'O and Josette Bellan. *Consistent Boundary Conditions for Multicomponent Real Gas Mixtures Based on Characteristic Waves.* Journal of Computational Physics, vol. 176, no. 2, pages 330–344, March 2002. (Cited on page 199.)

[Okong'O 2003] Nora Okong'O and Josette Bellan. *Real-Gas Effects on Mean Flow and Temporal Stability of Binary-Species Mixing Layers.* AIAA Journal, vol. 41, no. 12, pages 2429–2443, December 2003. (Cited on page 17.)

[Oppattaiyamath 2011] G. Oppattaiyamath, N. Reddy, S. Jammy and V. Kulkarni. *Conjugate Heat Transfer Analysis for Hypersonic Flow over Finite Thickness Flat Plate.* Journal of Aerospace Engineering, November 2011. (Cited on page 58.)

[Oschwald 1999] M. Oschwald. *Supercritical nitrogen free jet investigated by spontaneous Raman scattering.* Experiments in Fluids, vol. 27, pages 497–506, 1999. (Cited on page 12.)

[Oschwald 2002] M Oschwald and M. M. Micci. *Spreading angle and centerline variation of density of supercritical nitrogen jets.* Atomization and Sprays, vol. 11, pages 91–106, 2002. (Cited on page 12.)

[Oschwald 2006] M. Oschwald, J. J. Smith, R. Branam, J. Hussong, A. Schik, B. Chehroudi and D. Talley. *Injection of Fluids into Supercritical Environments.* Combust. Sci. Tech. , vol. 178, pages 49–100, 2006. (Cited on pages 12 and 41.)

[Palle 2007] Sridhar Palle and R.S. Miller. *Analysis of high-pressure hydrogen , methane , and heptane laminar diffusion flames: Thermal diffusion factor modeling.* Combustion and Flame, vol. 151, no. 4, pages 581–600, 2007. (Cited on page 197.)

[Pearson-Education 2011] Pearson-Education, 2011. (Cited on pages x and 29.)

[Pedot 2012] T. Pedot. *Modélisation du couplage thermique entre la combustion et l'encrassement des tubes d'un four de raffinerie.* PhD thesis, INP Toulouse, 2012. (Cited on pages 58 and 67.)

[Peng 1976] D.Y. Peng and D.B. Robinson. *A new two-constant equation of state.* Industrial and engineering chemistry fundamentals, vol. 15, pages 59–64, 1976. (Cited on pages 45 and 200.)

[Peters 1985] N. Peters. *Numerical and asymptotic analysis of systematically reduced reaction schemes for hydrocarbon flames.* In B. Larrouturou R. Glowinsky and R. Temam, editeurs, Numerical simulation of combustion phenomena, volume 241, pages 90–109. Springer-Verlag, Berlin, 1985. (Cited on page 80.)

[Petit 2013] X. Petit, G. Ribert, G. Lartigue and P. Domingo. *Large-eddy simulation of supercritical fluid injection.* The Journal of Supercritical Fluids, vol. 84, pages 61–73, 2013. (Cited on page 19.)

[Petit 2014] Xavier Petit. *Etude de l'interaction cinétique chimique/turbulence dans une flamme cryotechnique LOx/CH4.* PhD thesis, Coria, 2014. (Cited on page 51.)

[Pitzer 1955] K.S. Pitzer. *The volumetric and thermodynamic properties of fluids. 1. Theoretical basis.* Journal of the American Chemical Society, vol. 77(13), pages 3427–3433, 1955. (Cited on page 44.)

[Poinsot 1992] T. Poinsot and S. Lele. *Boundary conditions for direct simulations of compressible viscous flows.* J. Comput. Phys. , vol. 101, no. 1, pages 104–129, 1992. (Cited on pages 111 and 199.)

[Poinsot 2005] T. Poinsot and D. Veynante. Theoretical and numerical combustion. R.T. Edwards, 2nd edition, 2005. (Cited on pages 32 and 34.)

[Poitou 2011] D. Poitou, J. Amaya, M. ElHafi and B. Cuenot. *Analysis of the interaction between turbulent combustion and thermal radiation using unsteady coupled LES/DOM simulations.* Combustion and Flame, vol. 159, pages 1605–1618, 2011. (Cited on page 58.)

[Poling 2001] B.E. Poling, J.M. Prausnitz and J.P. O'Connel. The properties of gases and liquids. McGraw-Hill, 5th edition, 2001. (Cited on pages x, 41 and 49.)

[Pons 2009a] L. Pons, N. Darabiha, S. Candel, G. Ribert and V. Yang. *Mass transfer and combustion in transcritical non-premixed counterflows.* Combustion Theory and Modelling, vol. 13, no. 1, pages 57–81, 2009. (Cited on page 19.)

[Pons 2009b] L. Pons, N. Darabiha, S. Candel, T. Schmitt and B. Cuenot. *The structure of multidimensional strained flames under transcritical conditions.* Comptes rendus-Mécanique, vol. 337, no. 6-7, pages 517–527, 2009. (Cited on page 51.)

[Radenac 2005] E. Radenac, J. Gressier, P. Millan and A. Giovannini. *A Conservative coupling numerical method for transient conjugate heat transfer.* In In: International Conference on Computational Methods for Coupled Problems in Science and Engineering, Santorin, Greece, 25-28 May 2005. (Cited on page 62.)

[Radenac 2014] E. Radenac, J. Gressier and P. Millan. *Methodology of numerical coupling for transient conjugate heat transfer.* Computers & Fluids, vol. 100, pages 95–107, 2014. (Cited on page 62.)

[Rehab 1997] H. Rehab, E Villermaux and E.J. Hopfinger. *Flow regimes of large velocity ratio coaxial jets.* J. Fluid Mech. , 1997. (Cited on page 14.)

[Reid 1987] R. C. Reid, J. M. Prausnitz and B. E. Poling. The properties of gases and liquids. McGraw-Hill, 4th edition édition, 1987. (Cited on page 46.)

[Ribert 2008] G. Ribert, N. Zong, V. Yang, L. Pons, N. Darabiha and S. Candel. *Counterflow diffusion flames of general fluids: Oxygen/hydrogen mixtures.* Combustion and Flame, vol. 154, no. 3, pages 319–330, 2008. (Cited on pages 19 and 197.)

[Richard 2011] J. Richard and F. Nicoud. *Effect of the fluid structure coupling on the aeroacoustic instabilities of solid rocket motors.* In 17th AIAA/CEAS AeroAcoustics Conference, Portland, Oregon, USA, 2011. (Cited on page 58.)

[Ruiz 2011a] A. Ruiz, B. Cuenot, L. Selle and T. Poinsot. *The Flame Structure of a Turbulent Supercritical Hydrogen/Oxygen Flow Behind a Splitter Plate.* AIAA Paper 2011-6121, vol. 47th AIAA/ASME/SAE/ASEE Joint Propulsion Conference & Exhibit, 31 July - 03 August 2011. (Cited on page 20.)

[Ruiz 2011b] A Ruiz, T Schmitt, L Selle, B Cuenot and T Poinsot. *Effects of the Recess Length of a Coaxial Injector on a Transcritical LO2 / H2 Jet Flame.* In 23rd ICDERS, Irvine, CA, 2011. (Cited on pages xiv and 198.)

[Ruiz 2011c] A. Ruiz, T. Schmitt, L. Selle, B. Cuenot and T. Poinsot. *Effects of the Recess Length of a Coaxial Injector on a Transcritical LO2/H2 Jet Flame.* In 23rd ICDERS, Irvine, California, July 24-29 2011. (Cited on page 19.)

[Ruiz 2011d] A. Ruiz and L. Selle. *Simulation of a turbulent supercritical hydrogen/oxygen flow behind a splitter plate: cold flow and flame stabilization.* In 7th Mediterranean Combustion Symposium, Chia Laguna, Cagliari, Sardinia, Italy, 2011. (Cited on pages 197 and 209.)

[Ruiz 2012] A. Ruiz. *Unsteady Numerical Simulations of Transcritical Turbulent Combustion in Liquid Rocket Engines.* PhD thesis, Institut National Polytechnique de Toulouse, 2012. (Cited on pages x, 22, 53, 198 and 209.)

[Ruiz 2014] A. Ruiz, G. Lacaze, J.C. Oefelein, R. Mari, B. Cuenot, L. Selle and T. Poinsot. *A Numerical Benchmark for Validation of High-Reynolds Number Supercritical Flows with Large Density Gradients.* AIAA Journal, vol. Under review, 2014. (Cited on page 200.)

[Sagaut 2002] P. Sagaut. Large eddy simulation for incompressible flows. Springer, 2002. (Cited on page 36.)

[Saxena 2006] P. Saxena and F.A. Williams. *Testing a small detailed chemical-kinetic mechanism for the combustion of hydrogen and carbon monoxide.* Combust. Flame , vol. 145, pages 316–323, 2006. (Cited on page 200.)

[Schmitt 2009] T. Schmitt. *Simulation des grandes échelles de la combustion turbulente en régime supercritique.* PhD thesis, Université de Toulouse - Ecole doctorale MEGeP, CERFACS - CFD Team, Toulouse, June 2009. (Cited on pages 49, 51 and 52.)

[Schmitt 2010a] T. Schmitt, Y. Méry, M. Boileau and S. Candel. *Large-Eddy Simulation of oxygen/methane flames under transcritical conditions.* Proceedings of the Combustion Institute, vol. In Press, Corrected Proof, pages –, 2010. (Cited on pages x, 19, 21, 22 and 112.)

[Schmitt 2010b] T. Schmitt, L. Selle, A. Ruiz and B. Cuenot. *Large-Eddy Simulation of Supercritical-Pressure Round Jets.* AIAA Journal , vol. 48, no. 9, pages 2133–2144, September 2010. (Cited on pages 19, 112, 197 and 200.)

[Schumaker 2009] S.A. Schumaker and J.F. Driscoll. *Coaxial turbulent jet flames: Scaling relations for measured stoichiometric mixing lengths.* Proceedings of the Combustion Institute, vol. 32, no. 2, pages 1655–1662, 2009. (Cited on pages ix and 20.)

[Shankaran 2001] S. Shankaran, J.J. Alonso, M.F. Liou, N.S. Liu and R. Davis. *A Multi-Code-Coupling Interface for Combustor/Turbomachinery Simulations.* In 39th AIAA Aerospace Sciences Meeting and Exhibit, 2001. (Cited on page 58.)

[Singla 2005] G. Singla, P. Scouflaire, C. Rolon and S. Candel. *Transcritical oxygen/transcritical or supercritical methane combustion.* Proceedings of the Combustion Institute, vol. 30, no. 2, pages 2921–2928, 2005. (Cited on pages x, 21 and 22.)

[Singla 2006] G. Singla, P. Scouflaire, C. Rolon and S. Candel. *Planar laser-induced fluorescence of OH in high-pressure cryogenic LOx/GH2 jet flames.* Combustion and Flame, vol. 144, no. 1-2, pages 151–169, January 2006. (Cited on pages ix, xv, 15, 17, 18, 197, 217, 219, 220, 221 and 222.)

[Singla 2007] G. Singla, P. Scouflaire, J.C. Rolon and S. Candel. *Flame stabilization in high pressure LOx/GH2 and GCH4 combustion.* Proceedings of the Combustion Institute, vol. 31, no. 2, pages 2215–2222, January 2007. (Cited on pages 20 and 197.)

[Smagorinsky 1963] J. Smagorinsky. *General circulation experiments with the primitive equations: 1. The basic experiment.* Mon. Weather Rev. , vol. 91, pages 99–164, 1963. (Cited on page 36.)

[Smith 2000] G.P. Smith, , D.M. Golden, M. Frenklach, N.W. Moriarty, B. Eiteneer and M. Goldenberg. *GRI-Mech 3.0.* Rapport technique, 2000. (Cited on page 78.)

[Snecma 2011] Snecma. Vulcain 2 : Operating principle. 2011. (Cited on pages ix and 9.)

[Snyder 1997] R. Snyder, G. Herding, J. C. Rolon and S. Candel. *Analysis of Flame Patterns in Cryogenic Propellant Combustion.* Combustion Science and Technology, vol. 124, pages 331–370, 1997. (Cited on page 113.)

[Su 2006] L Su, O Sun and M Mungal. *Experimental investigation of stabilization mechanisms in turbulent, lifted jet diffusion flames.* Combustion and Flame, vol. 144, no. 3, pages 494–512, February 2006. (Cited on page 196.)

[Takahashi 1974] S. Takahashi. *Preparation of a Generalized Chart for the Diffusion Coefficients of Gases at High Pressures.* Journal of Chemical Engineering (Japan), vol. 7, no. 6, pages 417–420, 1974. (Cited on page 53.)

[Tsiolkovsky 1903] K. Tsiolkovsky. *The exploration of cosmic space by means of reaction devices.* 1903. (Cited on page 2.)

[Tucker 2008] P.K. Tucker, S. Menon, C.L. Merkle, J.C. Oefelein and V. Yang. *Validation of high-fidelity CFD simulations for rocket injector design.* In AAIA/ASME/SAE/ASEE Joint propulsion conference and exhibit, 2008. (Cited on page 19.)

[Valcke 2012] S. Valcke, V. Balaji, A. Craig, C. DeLuca, R. Dunlap, R. W. Ford, R. Jacob, J. Larson, R. O'Kuinghttons, G.D. Riley and M. Vertenstein. *Coupling technologies for Earth System Modelling.* Geoscientific Model Development, vol. 5, pages 1589–1596, 2012. (Cited on page 58.)

[Vargaftik 1975] N. B. Vargaftik. Tables on the thermophysical properties of liquids and gases. Wiley, New York, New York, 2nd édition, 1975. (Cited on page 47.)

[Villermaux 1998] E. Villermaux. *Mixing and Spray Formation in Coaxial Jets.* J. Prop. Power , vol. 14, pages 807–817, 1998. (Cited on page 14.)

[Villermaux 2000] E. Villermaux and H. Rehab. *Mixing in coaxial jets.* J. Fluid Mech. , vol. 425, pages 161–185, 2000. (Cited on page 14.)

[Westbrook 1981] C. Westbrook and F. Dryer. *Simplified reaction mechanism for the oxidation of hydrocarbon fuels in flames.* Combust. Sci. Tech. , vol. 27, pages 31–43, 1981. (Cited on page 79.)

[Yamashita 1996] H Yamashita, M Shimada and T Takeno. *A Numerical Study on Flame Stability at the Transition Point of Jet Diffusion Flames.* Proceedings of the Combustion Institute, vol. 26, no. 1, pages 27–34, 1996. (Cited on page 196.)

[Yang 2000] V. Yang. *Modeling of supercritical vaporization, mixing, and combustion processes in liquid-fueled propulsion systems.* PROCEEDINGS-COMBUSTION INSTITUTE, vol. 28, no. 1, pages 925–942, 2000. (Cited on page 17.)

[Yang 2004] V. Yang, M. Habiballah, J. Hulka and M. Popp. *Liquid rocket thrust chambers : aspects of modeling, analysis, and design.* American institue of Aeronautics and Astronautics, 2004. (Cited on pages ix, 9 and 10.)

[Yoo 2009] C. S. Yoo, R. Sankaran and J. H. Chen. *Three-dimensional direct numerical simulation of a turbulent lifted hydrogen jet flame in heated coflow: flame stabilization and structure.* Journal of Fluid Mechanics, vol. 640, page 453, December 2009. (Cited on page 196.)

[Zong 2004] Nan Zong, Hua Meng, Shih-Yang Hsieh and Vigor Yang. *A numerical study of cryogenic fluid injection and mixing under supercritical conditions.* Physics of Fluids, vol. 16, pages 4248–4261, December 2004. (Cited on page 19.)

[Zong 2006] N. Zong and V. Yang. *Cryogenic fluid jets and mixing layers in transcritical and supercritical environments.* Combust. Sci. Tech. , vol. 178, pages 193–227, 2006. (Cited on page 19.)

[Zong 2007] N. Zong and V. Yang. *Near-field flow and flame dynamics of LOX/methane shear-coaxial injector under supercritical conditions.* Proceedings of the Combustion Institute, vol. 31, no. 2, pages 2309–2317, 2007. (Cited on pages 19 and 197.)